

Article

Late Glacial Marine Transgression and Ecosystem Response in the Landlocked Elefsis Bay (Northern Saronikos Gulf, Greece)

Katerina Kouli ^{1,*}, Maria V. Triantaphyllou ¹, Olga Koukousioura ², Margarita D. Dimiza ¹, Constantine Parinos ³, Ioannis P. Panagiotopoulos ¹, Theodora Tsourou ¹, Alexandra Gogou ³, Nikolaos Mavrommatis ², George Syrides ², Styliani Kyrikou ¹, Elisavet Skampa ¹, Ester Skylaki ³, Christos Anagnostou ³ and Aristomenis P. Karageorgis ³

- ¹ Department of Geology and Geoenvironment, National and Kapodistrian University of Athens, Panepistimioupolis, 15784 Zografou, Greece; mtriant@geol.uoa.gr (M.V.T.); mdimiza@geol.uoa.gr (M.D.D.); ioapanag@geol.uoa.gr (I.P.P.); ttsourou@geol.uoa.gr (T.T.); skyrikou@geol.uoa.gr (S.K.); elskampa@geol.uoa.gr (E.S.)
- ² School of Geology, Aristotle University of Thessaloniki, 54124 Thessaloniki, Greece; okoukous@geo.auth.gr (O.K.); mavromm@geo.auth.gr (N.M.); syrides@geo.auth.gr (G.S.)
- ³ Hellenic Centre for Marine Research, Institute of Oceanography, 46.7 km Athens-Sounio Ave., 19013 Anavyssos, Greece; ksparinos@hcmr.gr (C.P.); agogou@hcmr.gr (A.G.); esterskilaki@gmail.com (E.S.); chanag@ath.hcmr.gr (C.A.); ak@hcmr.gr (A.P.K.)
- * Correspondence: akouli@geol.uoa.gr; Tel.: +30-210-7274896



Citation: Kouli, K.; Triantaphyllou, M.V.; Koukousioura, O.; Dimiza, M.D.; Parinos, C.; Panagiotopoulos, I.P.; Tsourou, T.; Gogou, A.; Mavrommatis, N.; Syrides, G.; et al. Late Glacial Marine Transgression and Ecosystem Response in the Landlocked Elefsis Bay (Northern Saronikos Gulf, Greece). *Water* **2021**, *13*, 1505. <https://doi.org/10.3390/w13111505>

Academic Editors: Serafeim E. Poulos, Vasilios Kapsimalis and Ioannis P. Panagiotopoulos

Received: 26 April 2021
Accepted: 21 May 2021
Published: 27 May 2021

Publisher's Note: MDPI stays neutral with regard to jurisdictional claims in published maps and institutional affiliations.



Copyright: © 2021 by the authors. Licensee MDPI, Basel, Switzerland. This article is an open access article distributed under the terms and conditions of the Creative Commons Attribution (CC BY) license (<https://creativecommons.org/licenses/by/4.0/>).

Abstract: Coastal landscapes are sensitive to changes due to the interplay between surface and submarine geological processes, climate variability, and relative sea level fluctuations. The sedimentary archives of such marginal areas record in detail the complex evolution of the paleoenvironment and the diachronic biota response. The Elefsis Bay is nowadays a landlocked shallow marine basin with restricted communication to the open Saronikos Gulf. A multi-proxy investigation of a high-resolution sediment core recovered from the deepest part of the basin offered a unique opportunity to record the paleoenvironmental and aquatic ecosystem response to climate and glacioeustatic sea level changes since the Late Glacial marine transgression. The retrieved sedimentary deposits, subjected to thorough palynological (pollen, non-pollen palynomorphs, dinoflagellates), micropaleontological (benthic foraminifera, calcareous nannoplankton, ostracods), and mollusc analyses, indicates isolation of the Elefsis Bay from the Saronikos Gulf and the occurrence of a shallow freshwater paleolake since at least 13,500 cal BP, while after 11,350 cal BP the transition towards lagoon conditions is evidenced. The marine transgression in the Elefsis Bay is dated at 7500 cal BP, marking the establishment of the modern marine realm.

Keywords: paleoenvironment; sea level rise; pollen spectra; dinoflagellate cysts; benthic foraminifera; calcareous nannoplankton; ostracods; molluscs; alkenone-based SSTs

1. Introduction

The complex Mediterranean coastal landscape includes rocky shorelines, bays, river deltas, coastal marshes, or lagoons, continuously shaped by geological processes, climate, and increasing human activity. Coastal areas, marginally located between land and sea, comprise a wide range of habitats and natural resources, thus, being continuously exploited by human populations since prehistoric times. The coastal zone is a dynamic environment, which is, however, particularly vulnerable in the context of global change [1] that has been dramatically transformed by the relative sea level changes in response to the Quaternary glacial/interglacial cycles (e.g., [2,3]).

Sedimentary records retrieved from coastal areas provide valuable evidence concerning past environmental changes, such as climate variability or sea level fluctuations, and ecosystem response. The study of such archives is critical for in-depth understanding

the forcing and the controlling processes in order to suggest the required adaptation and mitigation policies [4,5]. During the last decades, a big boost in the paleoenvironmental studies of coastal contexts is observed [6–18]. Coastal marshes and lagoons have been extensively investigated for their sedimentological, geochemical, micropaleontological, or palynological content in Greece, providing valuable knowledge concerning the evolution of their physical condition, the biota response to environmental shifts, and the impact of human activities on them (e.g., [14,19–22]). Changes in the micro- and macrofauna (foraminifera, ostracods, and gastropods) abundance, diversity, and species distribution can provide evidence of environmental factor fluctuations in water mass characteristics such as temperature, salinity, food availability, substrate, dissolved oxygen, and water quality [9,22–24]. The composition and distribution of phytoplankton (coccolithophores and dinoflagellates) are closely related to the conditions of the upper photic zone such as sea surface temperature, sea surface salinity, and nutrient availability, therefore their succession in the various Aegean Sea basins has been widely applied for the reconstruction of palaeoenvironmental conditions [25–30].

However, the coastal lagoon deposits suffer from deficiencies because their genesis is connected with the Holocene marine transgression and their sedimentary record mainly covers only the last 5000–8000 years [21,31,32]. During the Last Glacial, extensive areas were exposed [7,33,34] and, therefore, subject to erosion, because the sea level was ~120 m lower than present [35]. In contrast to lagoons, sedimentation processes continued in deeper coastal sites such as semi-enclosed gulfs and embayments. Being bounded by shallow sills, the gulfs of Saronikos, Amvrakikos, and Pagasitikos or the Gulf of Corinth became isolated during the glacial lowstand and reconnected to the Mediterranean Sea in the following /interglacial highstand cycle, while significant changes in sedimentary processes and environmental conditions were evidenced [36–42]. Elefsis Bay is a landlocked restricted shallow marine basin connected to the Saronikos Gulf by two shallow straits. The inner Saronikos Gulf, including Elefsis Bay, became isolated during the Last Glacial Maximum lowstand [37,43,44] and reconnected to the Aegean Sea during the Late Glacial–Holocene marine transgression. The metropolitan urban center of Attiki, one of the most populated areas in the Mediterranean, is located in the northern borderland of the inner Saronikos Gulf that receives the treated sewage of the entire region, whereas in Elefsis area significant industrial and shipbuilding activities take place. Following the Water Framework Directive 2000/60 concerning the ecological status of European waters [45], extensive research and continuous monitoring of the coastal water quality in Elefsis Bay has been conducted during the last decades, based on biotic and abiotic quality criteria [46–54].

This study applies systematic benthic foraminiferal, ostracod, calcareous nannoplankton, dinoflagellate cyst, and mollusc analyses, complemented by sedimentological analysis, selected lipid biomarkers, and absolute dating of the Late Glacial–Holocene Elefsis Bay deposits, aiming to investigate the temporal environmental conditions and decipher the role of the terrestrial and marine processes in the ecosystem, decode the response of the biota, and record the timing of the establishment of the marine environment in Elefsis Bay.

2. Regional Setting

Saronikos Gulf is a semi-enclosed neotectonic basin marked by low subsidence rates ranging from 0.03 to 0.31 m/ka [44] communicating to the south with the Aegean Sea and to the northwest with the Gulf of Corinth through the manmade Canal of Isthmus. The gulf is divided into a western and an eastern section by Methana, Angistri, Aegina, and Salamis islands (Figure 1), which are situated on a shallow N–S oriented platform. The western section of Saronikos Gulf comprises the deep (>400 m) Epidaurus Basin and the relatively shallow (<250 m) Megara Basin. The history of the eastern section of Saronikos Gulf reflects a low energy, shallow and rather stable marine basin throughout the Quaternary, with marginal faults at the northern and southern limits of Salamis basin displaying modest activity [55]. Several volcanoes and volcanic outcrops of Plio-Quaternary age, being part of the western active Aegean Volcanic Arc, are situated in the gulf [56].

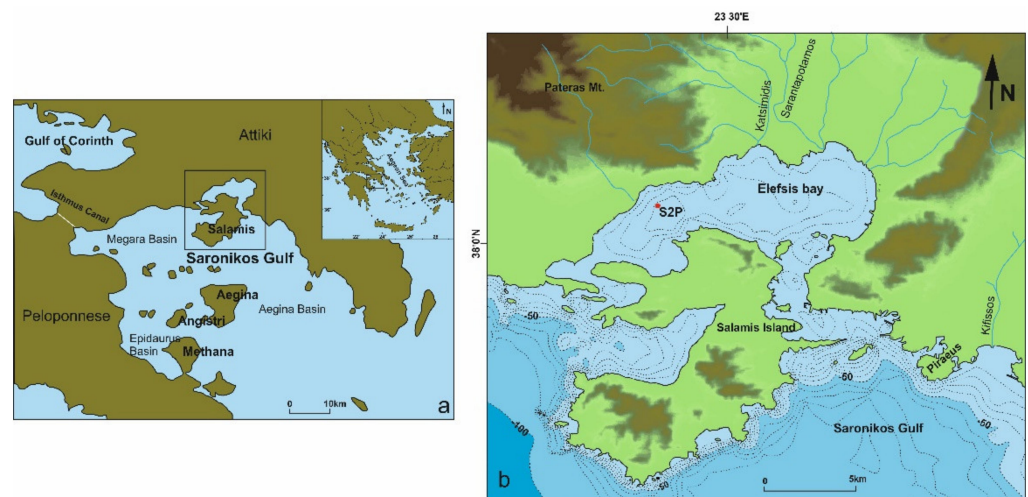


Figure 1. Location maps of the study area: (a) the Saronikos Gulf; and (b) the Elefsis Bay and the S2P coring location (source Hellenic Navy Hydrographic Service).

The Elefsis Bay lies in the northern part of Saronikos Gulf, covers an area of $\sim 68 \text{ km}^2$ and forms a natural embayment between western Attiki and Salamis Island (Figure 1). The bay is relatively shallow with a maximum depth of 33 m and communicates with the Saronikos Gulf through two straits, a western and an eastern one, having depths of 8 m and 12 m, respectively [43]. The water circulation is from west to east during summer, influenced by temperature difference between the water in the bay and the Saronic Gulf, while a reversed attenuated surface flow is recorded during winter, caused by differences in salinity [57]. The torrents of Sarantapotamos and Katsimidis, which drain the mountains of Pastra and Pateras, respectively, are the main sources of sediment and freshwater inputs to the basin [58]. Limestones and clastic sediments are found on land around the bay, associated with the Pliocene/Pleistocene substrate, while the Elefsis Plain is covered by recent post-alpine sediments, mostly talus, cones and scree [59].

The physical parameters of the water column in Elefsis Bay show a typical seasonal variation. The annual maximum temperature ($25 \text{ }^\circ\text{C}$) occurs during summer, while the minimum one ($10 \text{ }^\circ\text{C}$) is recorded in February/March. Salinity varies from 37.5 in March to 39 in summer (e.g., [60,61]). The reduced freshwater input and the restricted water mass exchange between the Elefsis Bay and Saronikos Gulf during summer leads to the development of a persistent thermocline down to a depth of 15 m. The dissolved oxygen stratification along the thermocline is also pronounced, featured by an upper layer ($<15 \text{ m}$) of oxygen supersaturation and consequent bottom water anoxia. During winter, an intense vertical mixing of the water masses occurs and the entire water column is enriched with oxygen (e.g., [51,62]). Finally, the trophic status of the Elefsis Bay is characterized as eutrophic [50,51], even though a general environmental improvement has been recorded over the last 30 years [63].

3. Materials and Methods

The gravity core S2P was recovered from the deepest part of Elefsis Bay ($38^\circ 00.50' \text{ N}$, $23^\circ 27.48' \text{ E}$; see Figure 1) at a depth of 35 m during an expedition with the R/V Aegaeo of the Hellenic Centre for Marine Research. The lithology and physical characteristics of the 342-cm-long core have already been presented by Petropoulos et al. [43]. Five major sedimentary units have been identified, based on their sand and biogenic debris content as well as their color (Figure 2): (i) the Unit A (0–192 cm), consists of light olive grey to olive grey mud with shell fragments; (ii) the Unit B (192–231 cm), mainly comprising grey clay; (iii) the Unit C (231–297 cm), demonstrates a variety of colors (yellowish, light grey, grey, dark grey, olive grey) and alternations of mud and sandy mud layers, while biogenic fragments occur within the upper portion of the bed; (iv) the Unit D (297–300 cm),

including an organic black sandy mud; and, finally, (v) the Unit E (300–342 cm), is composed of grey sandy mud with biogenic debris.

In addition to the previous sedimentological analysis, the relative proportion of sand and mud throughout the length of the core S2P was determined in detail by dry sieving of two hundred and thirty-one samples, while the total inorganic carbon (TIC) profile was derived by applying the equation of Jiang et al. [64].

3.1. Core Chronology

The chronostratigraphic framework of the core was defined using accelerator mass spectrometry (AMS) radiocarbon (^{14}C) dating, carried out in the Beta Analytic laboratory. The AMS ^{14}C dates were obtained from seven marine mollusc shells and one terrestrial plant material (Table 1). Calibration of the conventional ^{14}C ages to calendar years was made using the Marine13 calibration curve, by applying a ΔR correction of 73 ± 61 years for the marine reservoir effect in Piraeus (Saronikos Gulf), and the terrestrial IntCal13 calibration curve, respectively [65,66].

Table 1. AMS ^{14}C ages and reservoir-corrected¹ and calibrated ages for the S2P core.

Lab Code	Depth (cm)	Material	^{14}C yr BP	cal BP
Beta—496147	8–9	<i>Turritella communis</i>	970 \pm 30	451–563 ¹
Beta—441157	40–42	<i>Turritella communis</i>	2270 \pm 30	1706–1872 ¹
Beta—496148	70–72	<i>Turritella communis</i>	3930 \pm 30	3711–3904 ¹
Beta—441158	120–121	<i>Turritella communis</i>	4260 \pm 30	4179–4378 ¹
Beta—453192	155–156	<i>Turritella communis</i>	5840 \pm 30	6113–6268 ¹
Beta—453193	180–181	<i>Turritella communis</i>	6640 \pm 30	6992–7163 ¹
Beta—441159	242–244	<i>Cerastoderma glaucum</i>	10,220 \pm 30	11,083–11,218 ¹
Beta—441160	297–300	peat	11,650 \pm 40	13,439–13,496

¹ ΔR correction 73 ± 61 [65].

Finally, the age-depth model of the core was derived from the package rbacon [67] in the R console (v. 3.5.0).

3.2. Foraminifera and Ostracod Analysis

One hundred and fifty sediment samples (with the dry weight of each sample being 10 g) were treated with hydrogen peroxide (H_2O_2) solution 10% to remove the organic matter, washed through 63 μm and 125 μm stainless steel sieves and dried at 70 °C.

Seventy-two of the samples were analyzed for their benthic foraminiferal content in the >63 μm fraction. A subset containing at least 200 individuals per sample was obtained using an Otto microsampler. The individuals were identified under a Zeiss Stemi 305 stereoscope, following the generic classification of Loeblich and Tappan [68,69], and based on the studies of Cimerman and Langer [70], Hottinger et al. [71], Sgarrella and Moncharmont-Zei [72], and Dimiza et al. [73]. The total foraminiferal density (FD; number of specimens/g) and the relative abundances in the benthic foraminiferal assemblages were calculated. For samples containing less than 25 individuals, the countings were excluded from the quantitative analysis. Further, the Shannon–Wiener diversity index (H') was calculated, using the Past.exe 1.23 software package [74]. Additionally, all broken-reworked specimens were selected, without, however, being included in the counting.

Eventually, the >125 μm fraction in each of the one hundred and fifty samples was examined for the qualitative determination of its ostracod content. Ostracod species were identified under a Leica stereo microscope, based on the studies of Bonaduce et al. [75], Stambolidis [76], Tsourou [77], and Tsourou et al. [78].

3.3. Calcareous Nannoplankton Analysis

Seventy-five samples have been prepared for Calcareous Nannoplankton (CN), following the standard smear slide techniques. Out of them, only forty samples in the last 186 cm

of the core, were bearing CN assemblages. Detailed descriptions of the quantitative counting methods and taxonomy of CN analysis are presented in the studies of Triantaphyllou et al. and Triantaphyllou [25,26,79]. The results of the analysis are expressed as percentages in order to avoid any dilution effects, e.g., lithogenic input [80]. The variation in the joint abundance of *Helicosphaera carteri* and *Syracosphaera* spp. is used as a paleotracer of fresher upper water layer (e.g., [80–82]). *Helicosphaera carteri* has been reported exhibiting high frequencies in modern regions influenced by riverine discharge [83], as a coastal water taxon (e.g., [84]). Hints for an opportunistic behavior in estuarine environments, have been already given by Cachão et al. [10,85,86]. The abundances of reworked taxa from older sedimentary units are used as a lithogenic input proxy.

3.4. Palynological Analysis

One hundred and four samples were investigated via a meticulous palynological analysis. The samples were weighted, spiked, and chemically treated, following the standard palynological protocol including sieving through a 10 µm sieve (e.g., [87]). During the microscopic analysis, pollen, dinoflagellate cysts, green algae coenobia, and spores, as well as non-pollen palynomorphs (NPPs), were identified and counted. The six bottom samples of the S2P sedimentary sequence, corresponding to the 295–334 cm core-depth interval, were excluded from the analysis due to their low and poorly-preserved palynomorph content. An average of 300 pollen grains, excluding pollen from aquatics and spores, was counted in each of the ninety-eight examined samples [87], while dinoflagellate cysts were counted in approximately every second sample. An average of 120 dinoflagellate cysts was counted in each examined sample from the upper 247 cm of the core, while below that core depth only pollen, green algae, and NPPs were identified. The dinoflagellate cyst identification was based on the studies of Mudie et al. and Van Nieuwenhove et al. [88–90]. Cysts of the *Lingulodinium machaerophorum* with processes length shorter than 10 µm (*L. machaerophorum* sh.p.) were separately counted, based on the work of Mertens et al. [91,92]. Finally, the results derived from the analysis of pollen, dinoflagellate and NPPs are presented in both percentage and concentration diagrams.

3.5. Mollusc Analysis

The invertebrate specimens of the S2P core were retrieved from one hundred and forty-three samples, spaced at 1–3 cm core-depth intervals. Following the standard wet-sieving procedure, a maximum of 10 g of dry sediment from each sample was chemically treated with water-diluted H₂O₂ (Perhydrol, 30% v/v H₂O₂) and sieved through a 63 µm sieve. Treated samples were inspected under a Leitz Wetzlar stereo microscope and identified based on the WoRMs database [93], the MSIP database [94] and the study of Sakellariou [95]. The shell selection was based on the minimum number of individuals (MNI) criterion, while rounded/reworked specimens from specific core depths were also examined. Moreover, the collected specimens were distinguished to fresh or etched, depending on the shell conservation, which was considered as a paleoenvironmental condition parameter.

3.6. Organic Geochemistry

Selected lipid biomarkers, i.e., aliphatic hydrocarbons, long-chain alkenones and aliphatic alcohols, were determined in thirty-eight samples of the sedimentary Unit A as indices of paleoenvironmental conditions and land–sea interactions. Lipids were extracted from freeze-dried sediments by ultrasonication with a mixture of dichloromethane/methanol (4:1, v/v) and individual compounds were identified and quantified by means of gas chromatography, following Gogou et al. [96]. Estimates of past sea surface temperatures (SSTs) were made using the unsaturation ratios of alkenones (U^k₃₇) [97]. The U^k₃₇ index was converted into SST using the global calibration of Conte et al. [98]. High molecular weight odd-carbon number *n*-alkanes (*n*-C₂₇, *n*-C₂₉, *n*-C₃₁ and *n*-C₃₃) and even-carbon number *n*-alkanols (*n*-C₂₄, *n*-C₂₆, *n*-C₂₈ and *n*-C₃₀), major components of epicuticular higher plant waxes, are used as proxies of allochthonous natural (terrestrial) inputs [99,100]. The sums of

their concentrations are defined as ΣTerNA and $\Sigma\text{TerN-OH}$, respectively. Variations of the average chain length of terrestrial *n*-alkanes, i.e., ACL index [101], are commonly related to changes in the temperature and humidity/aridity in the growing environment, since plants tend to synthesize longer chain length waxes in response to elevated temperatures. The proportion of $\Sigma\text{TerN-OH}$ in the sum of ΣTerNA and $\Sigma\text{TerN-OH}$ (HPA index [101]) can be used to evaluate the proportions of labile and refractory organic matter delivered in the marine environment as well as in situ preservation vs degradation.

4. Results

4.1. Sedimentology/Age Depth Model

The mud fractions prevail in the S2P sedimentary record; however, increased sand content is observed within the 0–100 cm and 250–342 cm core-depth intervals (Figure 2).

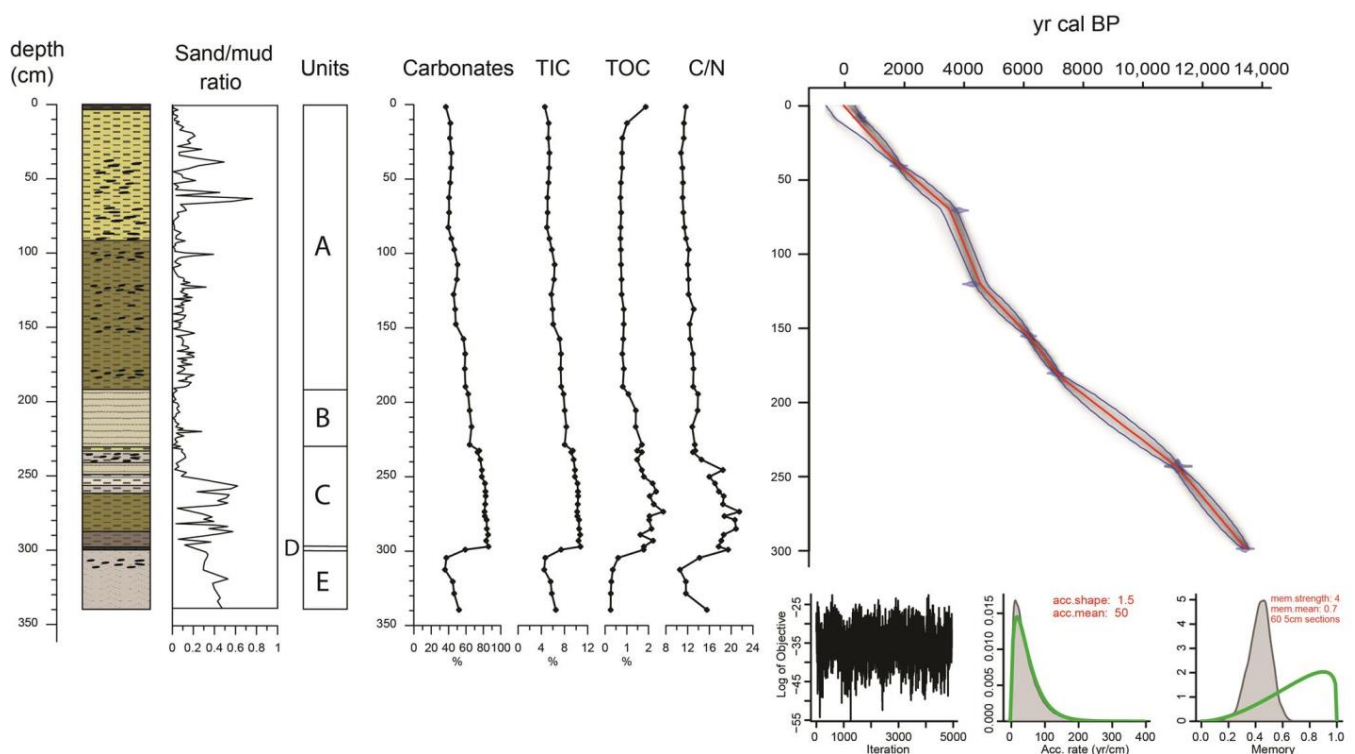


Figure 2. Physical characteristics of the core S2P, as have been already determined by Petropoulos et al. [43], and a Bayesian age-depth model (for the 0–297 cm core-depth interval) derived from the R package rbacon (see Blaauw and Christen [67]).

In the bottom Unit E, calcite layering is an outstanding feature, possibly indicating the substrate of the area that is most probably associated with the “Marls of Piraeus” considered of Pliocene age [102].

Upwards in Unit D, the occurring 3-cm-thick layer shows increased TOC values (~1.78%) despite its high sand content (Figure 2). This in combination with the black color of the sediment suggests a peat material, formed by incomplete decomposition of organic matter due to waterlogging and the subsequent anoxic condition. In addition, it is remarkable that Unit D disconformably overlies the eroded upper limit of Unit E (see photograph in Figure 4 of Petropoulos et al. [43]), thus, revealing a hiatus within the S2P depositional sequence. For this reason, a valid age-depth model for the S2P sequence could only be derived for the 0–300 cm core-depth interval, with the indicated ages ranging from 13,500 to 107 cal BP (see Figure 2).

TOC/ N_{total} ratios of pure marine organic matter are usually less than 8, while those between 8 and 12 indicate a mixed source of organic matter from land and sea [103]. Therefore, considering the relevant profile in Figure 2, Unit D and most of Unit C (248–297 cm) can be interpreted as terrestrial environments (C/N: 16–21.5), while the signal in Unit A

reveals a marine environment, which, however, is affected by terrestrial processes (C/N: 10.8–13). Eventually, Unit B and the rest of Unit C display C/N values (13–14.6) that imply a transitional depositional system, e.g., estuarine or lagoon.

Finally, in Unit A, the age model indicates a higher sedimentation rate at ~4000 cal BP (Figure 2). This could imply the occurrence of an upper shoreface depositional environment at that time.

4.2. Foraminiferal and Ostracod Analysis

The benthic foraminiferal assemblages in the S2P deposit are generally well preserved and a total of 67 species, belonging to 29 genera, were identified. The FD values demonstrate a high variability, ranging from 5 to 3908 specimens/g, while the H' index displays great fluctuations as well (0–2.76). The assemblages (see Figure 3) are mostly composed of *Ammonia beccarii*, *A. tepida*, *Aubignyna perlucida*, other small rotaliids (mainly *Nonionella turgida*, *Rosalina brady*, and *Planorbulina mediterraneensis*), bolivinids (mainly *Bolivina elongata*), elphidiids (mainly *Elphidium translucens* and *E. gunteri*), miliolids (mainly *Triloculina trigonula* and *T. tricarinata*), and agglutinant species (mainly *Textularia bocki* and *T. conica*).

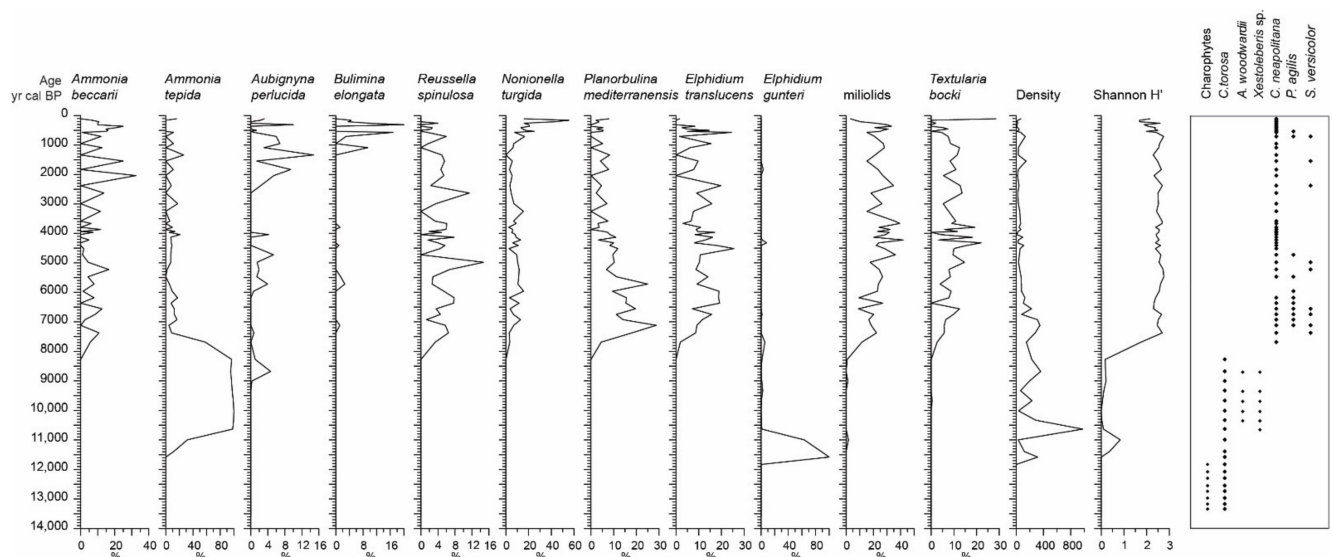


Figure 3. Profiles of the (i) relative abundances (%) of the most common benthic foraminiferal taxa, (ii) total foraminifera density, (iii) Shannon–Wiener diversity index (H') and (iv) qualitative charophyte and ostracod data in the S2P sedimentary sequence.

The interval from the bottom to 297 cm is characterized by the presence of calcified benthic foraminiferal specimens, mostly of *A. tepida*. The ostracod assemblage is characterized by the scarce presence of *Cyprideis torosa* calcified valves, which just below the peat material of Unit D (300–301 cm) occur in high numbers, exceeding 100 individuals/g. Other ostracod taxa, such as *Xestoleberis* and *Hiltermannicythere*, are also present, but are considered to be reworked.

Between 297 and 248 cm (13,500–11,350 cal BP), scarce *E. gunteri* specimens constitute the assemblage, being actually the only species observed in most samples (Figure 3). In this interval, only the upper two samples fulfilled the criterion to be included in the quantitative analysis, with *E. gunteri* appearing to be dominant and *A. tepida* showing a low abundance (11.6%). The FD parameter varies from 118 to 316 specimens/g, even though the H' index exhibits very low values (max 0.36). The ostracod assemblage is marked by the high occurrence of *C. torosa*, with many noded specimens (mainly juveniles), forming monospecific assemblages; in addition, charophytes were encountered.

Within 248–187 cm (11,350–7500 cal BP), an abrupt increase in *A. tepida* values is evidenced, exceeding 90% in the assemblage for the majority of the samples. *Elphidium*

gunteri shows a lower abundance, while *A. perlucida* and other small rotaliids, miliolids, and agglutinated taxa participate in the assemblage composition with minor values, mainly occurring within the upper part of the interval. The FD parameter demonstrates the highest values in the S2P sequence (max 977 specimens/g), while the H' index still presents a low level (max 1.75). In the same interval the ostracod assemblage are more diversified but they still remain oligospecific. *Cyprideis torosa* is the most abundant species, mainly accompanied by *Xestoleberis* sp., *Aurila woodwardii*, *Leptocythere lagunae*, and *Cytherois fischeri*.

From 187 cm to the top, a decrease in *A. tepida* values is observed. However, *A. beccarii* shows an enhanced abundance (max 32.4%), while each of the miliolid and small rotaliid assemblage constitute ~23% of the total assemblage, mainly represented by *T. trigonula*, *T. tricarinata* and *R. bradyi*, and *P. mediterraneensis* and *N. turgida*, respectively. In addition, *A. perlucida* (max 14.7%), *B. elongata* (max 20%), *E. translucens* (max 25.5%), and *T. bocki* (max 28.6%) contribute significantly to the microfauna composition, displaying a continuous presence and their highest values in the S2P core. Finally, the FD parameter decreases (71 specimens/g on average), while, in contrast, the H' index increases (2.44 on average). The ostracod assemblages demonstrate a completely different composition. *Cytheridea neapolitana* is the most abundant species, mainly accompanied by *Palmoconcha agilis*, *Leptocythere* spp. (primarily *L. multipunctata*), and *Sagmatocythere versicolor*. Finally, the fauna is characterized by the scarce presence of *Hiltermannicythere rubra*.

4.3. Calcareous Nannoplankton Analysis

All samples taken from Units B–E were barren of nannofossils. CN specimens begin to sporadically appear in the S2P record at 186 cm core depth, since ~7500 cal BP (Figure 4) and their assemblage is marked by a low number of species. *Emiliana huxleyi* is the dominant species throughout the studied interval (Figure 4), contributing to the total assemblage with frequencies up to 85%. *Rhabdosphaera clavigera* is the second most abundant species, representing 15%, on average, of the total coccolithophore assemblage. Its relative abundance varies between 5% and 18% during 7500–4000 cal BP (Figure 4), while afterwards shows an increase with a distinct peak (30%) centered at ~1300 cal BP and a relatively constant decreasing trend from 20% to less than 2% between 1000 and 100 cal BP. The distribution pattern of the species group *Helicosphaera carteri* + *Syracosphaera* spp. demonstrates relatively high values at ~7000 cal BP and between 3500 and 2000 cal BP (Figure 4). Finally, reworked taxa are present at low frequencies since 3800 cal BP, reaching their maximum abundances after 2000 cal BP with a prominent peak (up to 5%) at ~600 cal BP (Figure 4).

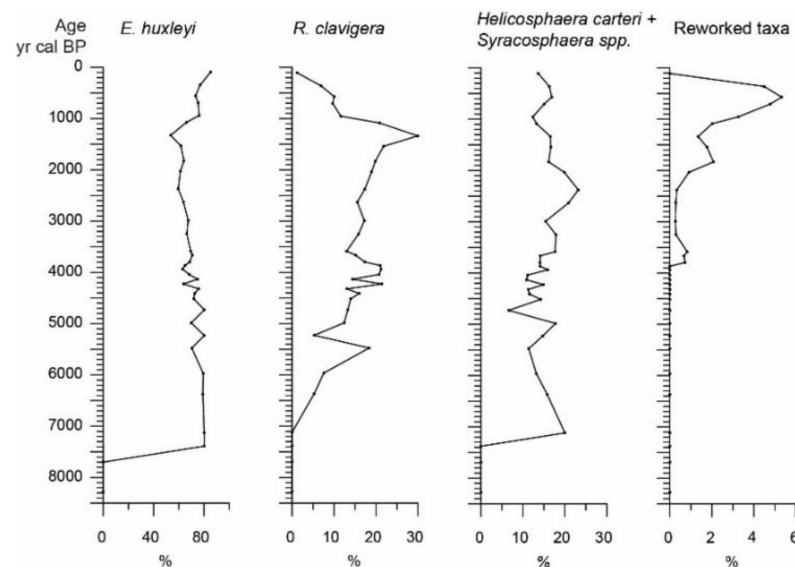


Figure 4. Abundance diagram of the Calcareous Nannoplankton assemblages in the S2P sedimentary sequence.

4.4. Palynological Analysis

The 0–300 cm interval of the S2P deposit yielded abundant pollen, dinoflagellate cysts, green algae, and other palynomorphs with significant temporal variability (see Figure 5). During the last 13,300 cal years BP the mean pollen concentration was 14,000 g/g (grains/g), while maximum values of 46,000 g/g were recorded at ~12,000 cal BP. A detailed description of the pollen assemblages and inferred vegetation development has already been presented in the study of Kyriku et al. [87]. Dinoflagellate cysts are continuously evidenced since 11,350 cal BP with a mean concentration of 6250 c/g (cysts/g), while green algae, mainly represented by *Botryococcus coenobia*, are present throughout the studied interval. Based on the aquatic palynomorphs encountered, three zones, i.e., PZ-I to PZ-III, may be determined, each one corresponding to a distinct palynomorph assemblage:

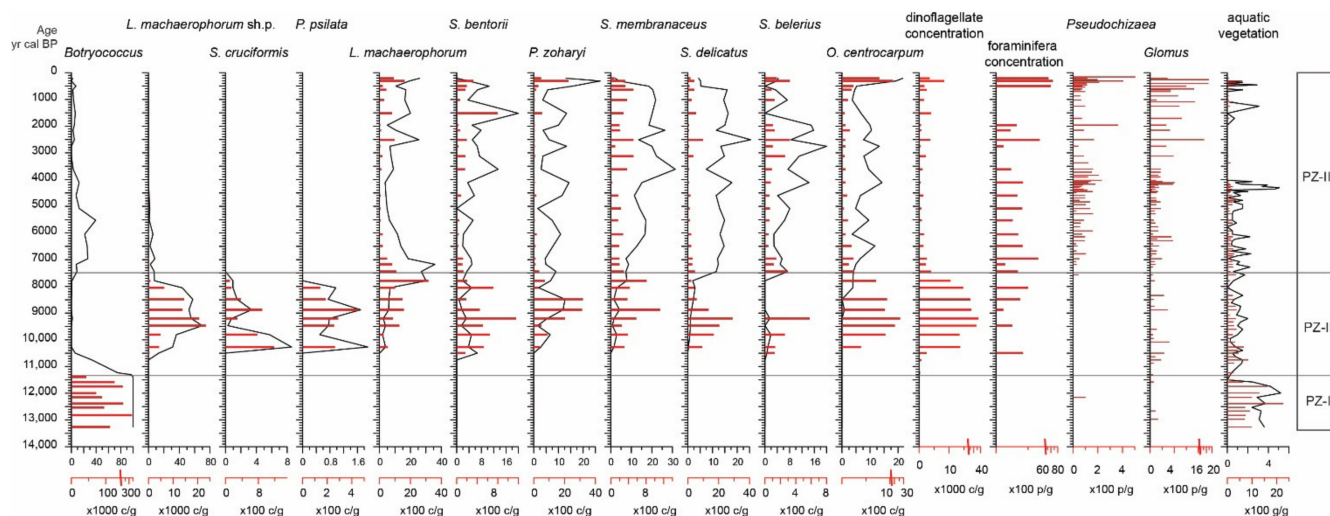


Figure 5. Percentage (line) and concentration (red bar) diagram of dinoflagellate cyst, green algae and other palynomorph assemblages in the S2P sedimentary sequence.

- (a) PZ-I (297–248 cm; 13,500–11,350 cal BP): *Botryococcus coenobia* are the dominant aquatic palynomorphs within this zone, displaying a mean concentration of 150,000 c/g (*coenobia*/g) and a distinct maximum concentration of 330,000 c/g. The mean concentration of aquatic vascular plants is 870 g/g, while dinoflagellate cysts are absent.
- (b) PZ-II (248–187 cm; 11,350–7500 cal BP): this zone is marked by a high dinoflagellate cyst concentration (15,300 c/g) and *Botryococcus* decrease to 320 c/g. The morphotype of *L. machaerophorum* sh.p. dominates the dinoflagellate assemblage (60%), which is complemented by *Spiniferites cruciformis* (mean of 3%, max 5.7%) and *Pyxidiniopsis psilata* (max 2%). The aquatic palynomorph assemblages are complemented by the long processes morphotype of *L. machaerophorum* (4%) and *S. bentorii* (3%). Foraminifera test linings are recorded for the first time in the record with a mean concentration of 780 p/g. A decrease in the aquatic vascular plant mean concentration (310 g/g) is also observed.
- (c) PZ-III (187–1.5 cm; 7500–158 cal BP): the dinoflagellate cyst and *Botryococcus* concentrations decrease to 3000 c/g and 180 c/g, respectively, while foraminifera test linings increase to 1550 p/g. The zone is characterized by a diverse dinoflagellate assemblage, including: *L. machaerophorum* (mean of 14%, max 35%, min 3%), *S. membranaceus* (16%), *S. delicatus* (13%), *Polysphaeridium zoharyi* (9%), and *Operculodinium centrocarpum* (9%). The *L. machaerophorum* sh.p. sharply decreases to 7% at the bottom of the zone and disappears after 4600 cal BP. The abundance of *Pinus*, both relative and absolute, gradually increases from the bottom of the zone, reaching maximum values since 3500 cal BP. Aquatic vascular plants are present until 4000 cal BP and reoccur after

1700 cal BP, while *Pseudoschizaeae* spores follow a similar pattern. Finally, after 2500 cal BP, *Glomus* reaches maximum concentrations of 1700 p/g.

4.5. Mollusc Analysis

A total of 10,500 mollusc specimens were collected, which resulted (MNI) in 7710 individuals (7251 fresh and 459 etched shells) belonging to 45 genera and 47 bivalve and gastropod species (see Figure 6).

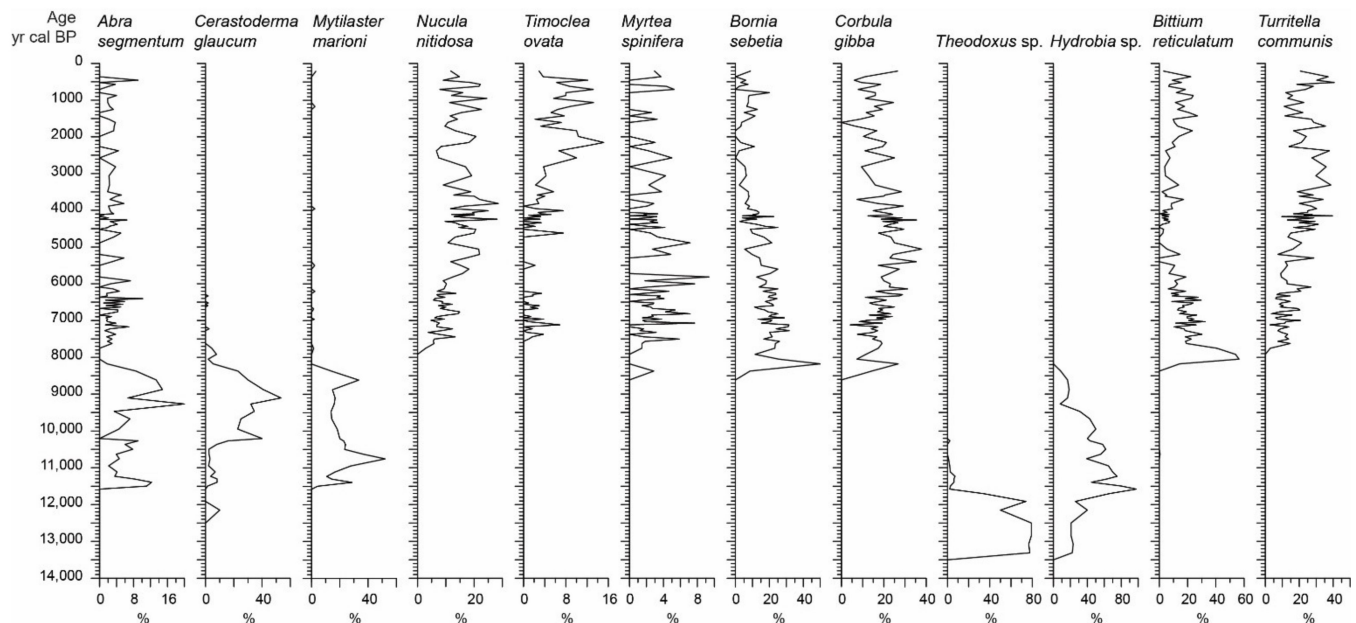


Figure 6. Relative abundances (%) of the most common mollusc taxa (bivalves and gastropods) in the S2P sedimentary sequence.

From the bottom to 297 cm the fauna includes exclusively rounded and possibly “fossilized” marine mollusc fragments, belonging mainly to bivalves but also to gastropods. Although the taxonomic attribution is not possible in a large amount of the specimens, some was possible to identify and they belong to *Cerastoderma*, Veneridae, *Loripes*, small Hydrobiidae, and few internal casts of hydrobiid gastropods. However, a few core-depth intervals showed a lack of any molluscan fauna.

Between 297 and 248 cm (13,500 to 11,350 cal BP), the monotonous fauna is dominated by the high abundances of the gastropods *Hydrobia* sp. (98.7–100%) and *Theodoxus* sp. (2.2–100%). The bivalve species *Cerastoderma glaucum* and *Mytilaster marioni* occur in two samples at 11,400 cal BP, showing, however, considerable values (max 10% and 28.6% of the total molluscan assemblage, respectively).

The 248–187 cm interval (11,350–7500 cal BP) is featured by the high occurrences of the bivalves *C. glaucum* (max 53.3%) and *Mytilaster marioni* (max 52%), and the gastropod *Hydrobia* sp. (max 75%). Occasionally, the bivalve *Abra segmentum* (max 20%) and the gastropod *Rissoa* sp. (max 24%) reach high values.

Finally, from 187 cm to the top (after 7500 cal BP), a rich variety of species is observed, including the dominant bivalves *Bornia sebetia*, *Corbula gibba*, *Myrtea spinifera*, *Nucula nitidosa*, and *Timoclea ovata*, and the gastropods *Bittium reticulatum* and *Turritella communis*. The previous species show abundances varying between 60% and 94% of the total assemblage.

4.6. Alkenone-Based SSTs and Paleoenvironmental Indices

The alkenone-derived SST measurements provide an average of 24.6 ± 0.8 °C, ranging from 22.3 to 25.7 °C. SSTs in Elefsis Bay increase (by ~1 °C) from 7500 to 7100 cal BP (Figure 7), reaching 25.2 °C at ~5500 cal BP and 25.7 °C at ~1600 cal BP, which is the highest value of the record. Afterwards, SST values decrease from 1300 to 600 cal BP (average

of 24.7 ± 0.3 °C), while a distinct decrease in SST is evident after 250 cal BP, reaching values as low as 22.3 °C (Figure 7). Σ TerNA and Σ TerN-OH concentrations present minor fluctuations from 7700 to 250 cal BP, with negative shifts at ~7500 and 4000 cal BP. Finally, an increasing trend is evident from ~1400 cal BP up to the top of the sequence.

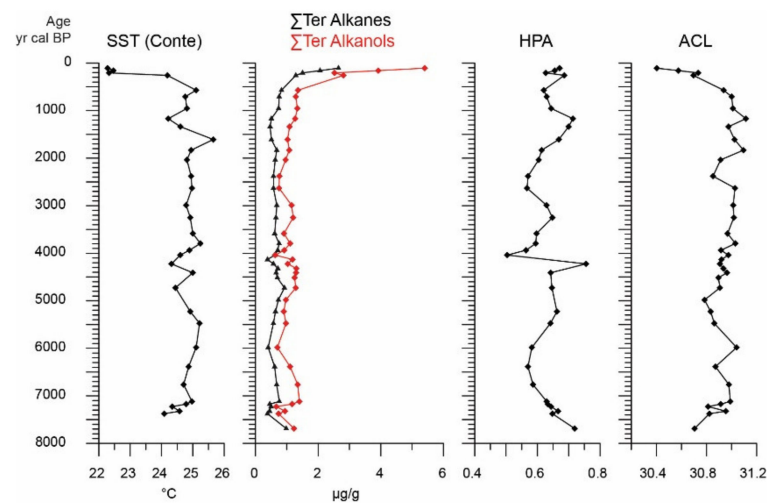


Figure 7. Profiles of alkenone-based SSTs as well as paleoenvironmental indices based on lipid biomarkers. Abbreviations are defined in the main text.

The HPA index sharply increases to 0.76 at 4200 cal BP, while an increasing trend, up to a 0.71, is also observed at ~1200 cal BP. Further, minor fluctuations around a value of 0.65 are noticed up to the top of the record. The ACL profile demonstrates an increasing trend from 7700 to 7100 cal BP and afterwards to ~5500 cal BP. Then, after a sharp reduction at ~2400 cal BP, ACL rises to 31.1 at ~1800 cal BP, displaying a secondary peak at ~1200 cal BP; the previous maxima are the highest of the record. Finally, ACL displays a distinct decline from ~700 cal BP towards the top of the sequence (Figure 7).

5. Paleoenvironmental Interpretation

The multi-proxy record derived from the S2P core sheds light on the temporal environmental variability in Elefsis Bay since the Late Glacial.

The investigated sequence starts with the sedimentary Unit E, which is featured by calcite layering. The most common process for the development of this feature is the one driven by microorganisms, e.g., blue-green algae, which grow in a tidal environment. These organisms flourish as filaments and form mats by trapping and binding microcrystalline carbonates during the incoming tides that sweep over the sand. This leads to the formation of calcite laminations that consist of organic tissue interbedded with mud [104]. Therefore, Unit E could reflect a tidal depositional system. This is further supported by the presence of heavily reworked and rounded mollusc fragments. These macrofossils rather represent material, which was most probably derived from the post-alpine sediments of the broader study area and, subsequently, reworked during its transport to the Elefsis Bay through the local torrents that drain the catchment area, while later, after its deposition in the tidal environment, it was subjected to further reworking and alteration. The timing of the deposition of Unit E was not feasible to be determined due to the lack of autochthonous biogenic material. However, the striking erosion surface on top of Unit E, revealing a well-defined disconformity with the overlying Unit D, implies that the depositional environment of Unit E could be a paleobeach, being significantly older than the rest of the S2P sequence.

Based on the results of the multidisciplinary analysis of the 0–300 cm interval of the S2P deposit, the paleoenvironmental evolution of the Elefsis Bay may be interpreted as follows.

5.1. Stratigraphic Interval of 300–248 cm: The Elefsis Paleolake (13,500–11,350 cal BP)

The postglacial sedimentation in Elefsis bay actually begins with the formation of the 3-cm-thick peat horizon (Unit D) at 13,500 cal BP.

Above this level, the occurring aragonite-rich sediment is dominated by the presence of the colonial freshwater green alga *Botryococcus* (see PZ-1 in Figure 5). *Botryococcus* coenobia are commonly found in freshwater lakes, even though they can tolerate salinities up to 8 [105,106]. The high concentrations of *Botryococcus* in this stratigraphic interval can be related with *green algae* blooms, suggesting the existence of a freshwater to oligohaline lacustrine depositional environment, probably associated with the paleolake of Kyrheia [107]. In addition, the high relative and absolute abundances of pollen originating from terrestrial aquatic plants (see Figure 5) support the interpretation for the establishment of wetland conditions in the bottom part of the suggested paleolake environment, which, consequently, explains the peat formation. According to the glacio-hydro-isostatic model of Lambeck [3], the sea level stand was -80 m at 13,000 yr BP and -57 m at 11,000 yr BP, apparently favoring the formation of a paleolake within the enclosed depression of Elefsis.

In the current interval, the high TOC and C/N values (see Figures 2 and 8) are indicative of a terrestrial origin of the organic matter, while the recorded aragonite enrichment [4] suggests a shallow freshwater environment of high productivity and sulphate reduction [108]. Also, a typical inorganic precipitation of calcium carbonate in the form of aragonite frequently occurs in freshwater bodies affected by salinity increments. Hence, all previous interpretations as well as the pronounced rise in the carbonate contents (see Figure 2) further support the perception of a freshwater to oligohaline depositional environment for this sediment.

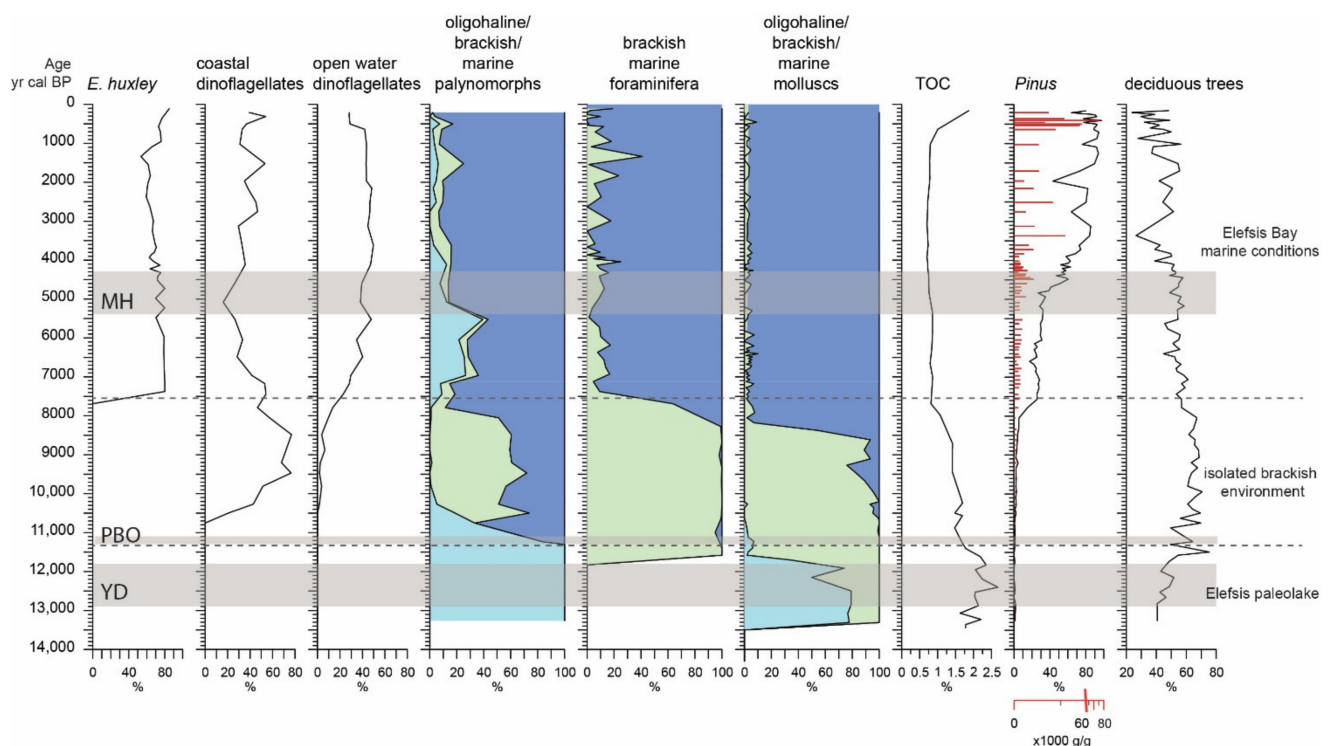


Figure 8. Paleoenvironmental interpretation of the S2P sedimentary sequence. Younger Dryas (YD), Preboreal oscillation (PBO), and Mid-Holocene warm period (MH) climatic intervals are marked with grey bands. Light blue: oligohaline/fresh water, green: brackish, navy blue: marine assemblages.

The gastropod *Theodoxus* sp., often associated with “hard” water [109], is the main mollusc species encountered within the present interval (see Figure 6). Thus, this is an extra indication of low salinity to freshwater conditions. Such conditions are also concluded from the coeval presence of perolithosis elements, etched specimens, and charophytes that

never occur in marine habitats or under long-term conditions of high salinity, but they are usually found in freshwater and brackish water bodies [110].

Only the scarce occurrence of the foraminifer *Elphidium gunteri* was recorded during most of this stratigraphic interval (Figure 3). However, after 11,580 cal BP an evident increase of the FD values is observed, characterized by the concomitant presence of *E. gunteri* and *Ammonia tepida*. *Elphidium gunteri* is a common and, sometimes, dominant species in marshes and brackish lagoons and waters [23,111–113], which is, however, capable not only surviving but even thriving in lacustrine environments of extremely low salinities (even <2) [114]. Also, it is generally recorded in intertidal environments along with *A. tepida*, which is an euryhaline opportunistic taxon exceptionally tolerant in salinity and temperature fluctuations [115,116]. Therefore, the simultaneous increased occurrence of the previous species in the current stratigraphic interval should be related to a high abundance of blue-green algae since the aforementioned species feed on these algae [117]. This actually reflects a very low salinity paleoenvironment [118].

More evidence that an oligohaline and shallow depositional environment had developed during this interval is further provided by the identified abundant monospecific assemblage of the ostracod species *C. torosa* with many noded individuals (see Section 4.2), which is a reliable indicator of such an environment. In detail, *C. torosa* is highly euryhaline and common in brackish waters showing an adaptability ranging from oligohaline to hypersaline waters [119], while dense assemblage of the species occur when salinity fluctuates between 2 and 17 [120]. Noded valves of *C. torosa* represent an ecologically-driven phenotypic variability developing under very low salinities [121]. In particular, nodes are usually present when salinity is less than 14, while more than 20% of noded valves point to a salinity of less than 5 [122].

The development of the Elefsis paleolake is further validated by the Late Glacial terrestrial vegetation succession in the area. The presence of well-developed open thermophilous deciduous and Mediterranean evergreen woodlands, implies relatively wet and mild climatic conditions in the Elefsis region during c.a. 13,500–11,500 cal BP [87]. Such relatively humid conditions are also supported by the occurrence of the continuous and extensive aquatic vegetation around the paleolake (see Figure 5) as well as the high abundances of the hydrophilous big Poaceae, recorded by Kyrikou et al. [87]. Interestingly, the Younger Dryas climatic event interval (12,900–11,700 cal BP; [123]), documented as a cold and arid period in the Aegean records [124,125] and terrestrial sites from northern Greece [126,127], coincides with the Elefsis paleolake phase. However, there is no signs of increasing aridity in the high-resolution Elefsis paleovegetation record [87], indicating the occurrence of milder conditions in south Greece. Increased humidity in southern sites across the Hellenic peninsula during the Younger Dryas is also supported by the glacial record of Chelmos Mountain (in Peloponnese) [128] compared to that of Pindus Mountain Range [129–131].

5.2. Stratigraphic Interval of 248–187 cm: The Isolated Brackish Environment (11,350–7500 cal BP)

After 11,350 cal BP, a shift in the aquatic biota assemblages is evidenced as new taxa are introduced and the concentrations of the green algae *Botryococcus* abruptly decline (see PZ-II in Figure 5). A distinct dinoflagellate assemblage, dominated by *L. machaerophorum* sh.p. and complemented by *S. cruciformis* and *Pyxidiniopsis psilata*, is recorded, indicating the establishment of brackish conditions in the area. These autotrophic species are known from brackish deposits in the Black and Caspian seas [30,88,132] and are common in low salinity environments [133]. *Lingulodinium machaerophorum* is known to have a widespread distribution in coastal environments with increased river discharges [88]. The *L. machaerophorum* sh.p., with length of processes <10 µm, is typical of waters with reduced sea surface salinity (SSS) [88,92,134], associated with annual SSTs of ~17–20 C and SSS values of ~12.4–13.2 [88]. *Spiniferites cruciformis* is a cyst found in the Eastern Mediterranean, mainly restricted to areas of the Black and Caspian seas with reduced salinity affected by river discharges [30,88,133,134], but also recorded in lacustrine deposits [28]. Comparable low diversity assemblages of *S. cruciformis*, *P. psilata* and *L. machaerophorum* sh.p. have

already been recorded in the isolated/semi-isolated intervals of the sedimentary record obtained from the Gulf of Corinth during the IODP Expedition 381 [39,135]. Finally, the typical brackish assemblage of this stratigraphic interval is complemented by some euryhaline species, such as *S. bentorii* and *P. zoharyi*, which thrive in coastal environments [133].

In accordance to the interpretation inferred from the dinoflagellate analysis, the relatively increased C/N values (13–14.6) in the current interval further support the establishment of a transitional environment [103]. In addition, eutrophic conditions associated with riverine inputs can be inferred from the enhanced TOC values as well as the peak dinocyst concentration, most likely related to bloom conditions of the *L. machaeorophorum* [88,136], known for its flourishing in nutrient-rich environments. Towards the top of PZ-II, the gradual introduction of *S. membranaceus*, *S. delicatus*, and *O. centrocarpum* (see Figure 5) indicates a deepening of the suggested lagoon environment. The previous interpretation is further strengthened by the retreat of aquatic vegetation as a result of the reduction of the shallow areas.

In this stratigraphic interval, the foraminiferal assemblage (Figure 3) is highly dominated by the euryhaline species *A. tepida*, accompanied by *A. perlucida* and *E. gunteri*, displaying low diversities but high FD values. The dominance of *A. tepida* is consistent with its tolerance to decreased marine influence [137], while the occurrences of *A. perlucida* and *E. gunteri*, together with the presence of *A. tepida*, suggest an environment of low salinity and/or intense salinity fluctuation, thus, revealing typical conditions of an inner lagoon or an isolated brackish waterbody [22,23,32,138–140]. As has been observed by Melis and Covelli [113], the muddy composition and high organic matter content could explain the high density and dominance of *A. tepida* in this stratigraphic interval, taking also into account that the organic matter is a vital food resource for *A. tepida* [141].

More evidence that lagoonal conditions had prevailed during the present interval is further provided by the identified ostracod assemblage (see Section 4.2). It is primarily composed of *C. torosa*, with rare presence of noded juvenile valves, accompanied by *Xestoleberis* sp. The *Xestoleberis* species are abundant in shallow marine environments and are highly associated with algae [142,143]; however, several *Xestoleberis* species have been recorded in brackish marine environments with submerged aquatic vegetation (e.g., [144]). Even though other ostracod species are scarcely present in the current stratigraphic interval, the identified individuals reflect brackish conditions. For example: *A. woodwardii* is a marine littoral epibenthic and epiphytal species [77,145], found also in brackish lagoonal environments [146]; *L. lagunae* is considered as a marine littoral species, being common in lagoonal systems (e.g., [147]); and *C. fischeri* is a brackish water marine littoral species, tolerating a wide range of salinities (4–35) [148,149].

Eventually, lagoonal conditions are interpreted by the molluscan fauna analysis too. The molluscan assemblage are characterized by the typical euryhaline bivalve *C. glaucum* (see Figure 6) being common in shallow oligohaline lagoons [150,151], *M. marioni* preferring brackish environments [152], *Hydrobia* sp. known to live in salinity levels that range from brackish to freshwater [6], and *Abra segmentum* thriving in silty oligohaline lagoons [153,154]. Therefore, based on the particular features of the previously mentioned assemblage, an inner lagoon depositional system of low salinity conditions is indicated [138,155–160].

The evolution of the Elefsis paleolake into an isolated brackish waterbody is the result of the Early Holocene gradual marine transgression that caused a relative sea level rise from –57 m at 11,000 yr BP to –13.5 m at 7500 yr BP, as predicted by the glacio-hydro-isostatic model of Lambeck [3]. However, the shallow depth at the sills occurring in the western and eastern strait, respectively, actually prevented the seawater masses to inundate the Elefsis embayment. That might be the reason that we have not found any calcareous nannoplankton representatives during this interval, although their progressive increase in abundance could be of importance when characterizing the establishment of lagoonal conditions (e.g., [8]). Hence, we believe that the prevailing brackish lagoonal environment was not established via a direct connection with the sea but due to a potential salinization caused

by lateral seawater intrusion processes as the sea level was constantly rising (e.g., [161]). The beginning of this isolated brackish phase with evidences of increasing riverine input is also featured by short-lived fluctuation in the abundance of deciduous trees (Figure 8) and decline of Mediterranean elements in Elefsis pollen record [87] associated to the Preboreal oscillation interval (PBO). Similar temporal setbacks of forest expansion evidenced in several Mediterranean sites [124,126,162,163] are likely driven by changes in temperature and seasonal precipitation [164,165].

5.3. Stratigraphic Interval of 187 cm to the Top: The Elefsis Bay (7500 cal BP to Present)

The establishment of marine conditions in the Elefsis Bay is marked by the development of diverse dinoflagellate, benthic foraminiferal, and mollusc assemblages at 7500 cal BP as well as the introduction of coccolithophores in the assemblages (Figures 3–6). The dinoflagellate assemblage is characterized by a sharp decrease of the low salinity species and the development of a marine assemblage consisting mainly of *L. machaerophorum*, *Sp. Bentorii*, and *P. zoharyi* (see PZ-III in Figure 5). In particular, the high abundances of the long processes morphotype of *L. machaerophorum* and the co-occurrence of *P. zoharyi*, *S. bertonii*, and *S. belerius* at the bottom of this interval (see PZ-III Figure 5) are indicative of a coastal environment enriched in nutrients due to enhanced terrestrial discharges [88,136,166,167]. The dinocyst assemblage becomes gradually enriched with pelagic species, such as *Sp. delicatus*, *S. membranaceus*, *S. mirabilis*, and *O. centrocarpum*, evidencing the deepening of the marine environment (Figure 8). The contemporaneous occurrence of *E. huxleyi* in the sedimentary record (Figure 4) implies the establishment of full marine conditions in the Elefsis Bay, with a sufficient water column depth, i.e., at least 20 m, to sustain the pelagic coccolithophore community (e.g., [168]), conditions that coincide with the increase of pelagic environment dinoflagellate cysts (see Figure 8). Likewise, in benthic communities the marine transgression is featured by a sudden increase in diversity and the appearance of several marine species in the foraminiferal, ostracod, and molluscan assemblages; the latter comprising several typical marine gastropod and bivalve species, such as *B. sebetia*, *N. nitidosa*, *T. ovata*, *B. reticulatum*, and *T. communis*. The benthic foraminiferal composition until 4000 cal BP (Figure 3) mainly includes typical marine species of the infralittoral zone, such as *A. beccarii*, small epiphytic rotaliids, *E. translucens*, miliolids, and agglutinated taxa [72,111,169], similar to modern coastal environments of the Aegean Sea [23,73]. The abundance of the euryhaline *A. tepida* dramatically decreases, while *A. beccarii* appears together with shallow-water epiphytic foraminifera, such as *P. mediterraneensis*, *R. spinulosa*, and *T. bocki*, common in the infralittoral and circalittoral zones of the Mediterranean Sea [72,170,171]. Similarly, the ostracod fauna comprises the typical marine species of *C. neapolitana*, *P. agilis*, *S. versicolor*, and *L. multipunctata* (e.g., [75,77,145,172]). In particular, *C. neapolitana* being the most abundant in the ostracod assemblages, indicates water depths higher than 20 m, tolerating organic matter enrichment and oxygen depletion [173,174].

More evidence for the development of a marine basin after 7500 cal BP is provided by the relative and absolute abundances of *Pinus* pollen (Figure 8). *Pinus* pollen is mostly overrepresented in offshore deposits [175–177] and, therefore, is commonly excluded from the analyses of marine pollen records [79,124,165,178–180]. Even in the large terrestrial water body of Lake Ohrid, pine is considered overrepresented (e.g., [181]), while its gradual increase over the earliest lake stages has been connected with the increase of the lake surface area [182]. Despite the fact that pine is a significant component of the Mediterranean vegetation, its marked occurrence in the marine stratigraphic interval of the S2P record is most probably attributed to depositional processes and not to an expansion of the species in the borderlands of Elefsis Bay [87]. Thus, the observed abrupt, pine increase can be correlated with the marine transgression in the bay at 7500 cal BP.

The change in the paleoenvironmental conditions is clearly displayed in the C/N values (see Figure 2), which diminish to 12.2–13 in the lower part of this stratigraphic interval, indicating the establishment of a marine environment significantly affected by the terrestrial processes that, however, appear less effective after 4000 cal BP [103]. In agreement

with the previous interpretation, the increased concentrations of the erosion indicating *Glomus* and *Pseudoschizaea* signal constant terrestrial runoff [183] culminating between 5000 to 4000 cal BP. The terrestrial inputs are further documented by the relatively elevated ΣTerNA and $\Sigma\text{TerN-OH}$ concentrations and the high HPA values in the same time interval; the biomarkers evidence low degradation of terrigenous organic matter likely associated with enhanced freshwater inputs/land runoff, delivering “fresh” land plant organic matter (e.g., [96,184]). The persisting abundances of the green alga *Botryococcus* and the occurrence of the low-salinity *L. machaerophorum* sh.p. until 4600 cal BP provide additional evidence for seasonal freshwater fluxes into the basin [88,136], during a period of ongoing warm and humid paleoclimatic conditions associated with the Mid-Holocene warm period (5400–4300 cal BP; [25,184]) in the Aegean Sea (Figure 8), as marked by the increment of the ACL index indicating vegetation shift towards “warmer species”. This phase ends with the “4.2 ka” significant Northern Hemisphere rapid climate cooling [185,186] that is also evidenced as negative shift in the SST profile of S2P record (Figure 7).

The prominent HPA minimum at ca. 4000 cal BP in line with a decrease in ΣTerNA and $\Sigma\text{TerN-OH}$ concentrations (Figure 7) and the decline of the aquatic vegetation (Figure 5) mark the onset of an arid period. The simultaneous increase in the abundance of *S. membranaceus* after 4000 cal BP verifies the changes in the marine environment. The species is known to be abundant in mesotrophic to oligotrophic environments [88,187], therefore its enhanced occurrence most probably implies a decline in the trophic status, also reflected in the lower TOC values during the same interval. The simultaneous scarcity of the erosion indicators *Glomus* and *Pseudoschizaea* suggests a reduction in the terrestrial runoff, related with increasing aridity recorded in a plethora of regional terrestrial and marine archives (e.g., [25,188–190]).

At the uppermost part of the S2P sequence, the establishment of the present-day conditions, characterized by dysoxic/anoxic conditions, restricted circulation, and increased terrigenous runoff [183], is reflected in all applied proxies. In regard to the benthic foraminiferal communities, these are characterized after 1500 cal BP by the peak values of *B. elongata* and the mud-dwelling *N. turgida* [191]. Both species are known to thrive in silty to sandy substrates under the influence of ample inputs of fluvial organic matter and sediment [191–193], and even to survive in dysoxic habitats [111,194,195]. Furthermore, the organic enrichment of the environment is implied by the presence of the tolerant in dysoxic conditions bivalves *C. gibba*, *M. spinifera*, and *T. ovata* [196–199]. Hence, the contemporaneous increase of ΣTerNA and $\Sigma\text{TerN-OH}$ contents, high HPA values and the minima in the ACL profile after 1500 cal BP (Figure 7) should be mostly linked to the enhanced freshwater supply and subsequent stratification/oxygen depletion in the marine water column that promotes in-situ preservation (e.g., [96,200]).

Finally, the gradual increase of the dinocysts *L. machaerophorum*, *S. bentorii*, and *P. zoharyi* as well as the maxima in the *Pseudoschizaea* and *Glomus* concentration profiles are most probably correlated to enhanced fluvial inputs to the basin [88,187], which are further supported by the enhanced abundance of CN reworked taxa (e.g., [25]).

6. Conclusions

The multi-proxy analysis of the Elefsis Bay sedimentary record provides insights into the sensitive response of marginal aquatic ecosystems to the environmental variability linked to sea level changes and the Late Glacial marine transgression. Marked shifts in benthic and planktic biota assemblages, complemented by geochemical data, were identified, featuring the paleoenvironmental evolution of this shallow landlocked marine area:

- The bottom part of the S2P sequence, most probably representing the Pliocene/Pleistocene substrate of the area, was rather deposited in a tidal system as implied by the presence of calcite layering and heavily reworked and rounded mollusc fragments. A well-defined disconformity with the rest of the sequence is recorded.

- Between 13,500 and 11,350 cal BP, a freshwater to oligohaline lacustrine environment developed, i.e., the Elefsis paleolake, characterized by green algae blooms and monospecific ostracod and gastropod oligohaline faunas.
- The occurrence of an isolated brackish environment is evidenced after 11,350 cal BP by a marked shift in the aquatic biota. Brackish dinoflagellate assemblages, mainly composed of low salinity morphotypes of *L. machaerophorum*, replace the green algae in the assemblages. In parallel, benthic communities are featured by high foraminiferal density values of the euryhaline species *A. tepida*, *A. perlucida*, and *E. gunteri*, while the prevailing ostracods *C. torosa* and *Xestoleberis* sp. together with the molluscs *C. glaucum*, *M. marioni*, and *Hydrobia* sp. imply an inner lagoon depositional system. As the Early Holocene relative sea level stand was not high enough to allow a direct communication of the Elefsis waterbody with the sea, the established brackish conditions were most probably the result of salinization caused by lateral encroachment from coastal waters.
- The marine conditions in Elefsis Bay are established after 7500 cal BP, evidenced by the development of a diverse dinoflagellate assemblage, gradually enriched with pelagic species, and the contemporaneous occurrence of calcareous nannoplankton assemblages, dominated by *E. huxleyi*. In the benthic communities the marine transgression is reflected by a sudden increase in the foraminiferal diversity and the appearance of several marine species.
- After 1500 cal BP, both benthic foraminiferal and bivalve communities are dominated by taxa tolerant in dysoxic conditions, suggesting organic matter preservation. In accordance, the contemporaneous increase of ΣTerNA and $\Sigma\text{TerN-OH}$ content, high HPA values as well as the minima in the ACL profile are linked to an enhanced freshwater supply and subsequent stratification/oxygen depletion in the marine water column, implying the earliest establishment of the present-day seasonal anoxia in the Elefsis Bay.

Author Contributions: Conceptualization, K.K., M.V.T., O.K., and C.A.; methodology, K.K., O.K., M.D.D., I.P.P., G.S., and C.P.; investigation, K.K., O.K., T.T., M.V.T., N.M., S.K., C.P., and E.S. (Ester Skylaki); data curation, K.K., O.K., and E.S. (Elisavet Skampa); writing—original draft preparation, K.K., M.V.T., O.K., and M.D.D.; writing—review and editing, I.P.P., G.S., T.T., A.G., N.M., C.A., and A.P.K.; visualization, K.K., O.K., T.T., and E.S. (Elisavet Skampa); project administration, A.P.K. All authors have read and agreed to the published version of the manuscript.

Funding: This research was funded by the European project “Policy-oriented Marine Environmental Research in the Southern European Seas” (PERSEUS, EC 7th FP), grant number GA 287600 and the Greek National Project CLIMPACT: Flagship Initiative for Climate Change and its Impact by the Hellenic Network of Agencies for Climate Impact Mitigation and Adaptation. KRIPIS—Integrated Observatories in the Greek Seas, grant number MIS 451724 is acknowledged for the absolute datings. The work of SK was funded by the NKUA grant 13014.

Institutional Review Board Statement: Not applicable.

Informed Consent Statement: Not applicable.

Data Availability Statement: The data presented in this study are available on request from the corresponding author.

Conflicts of Interest: The authors declare no conflict of interest.

References

1. Giorgi, F.; Lionello, P. Climate change projections for the Mediterranean region. *Glob. Planet. Chang.* **2008**, *63*, 90–104. [[CrossRef](#)]
2. Siddall, M.; Rohling, E.J.; Almogi-Labin, A.; Hemleben, C.; Meischner, D.; Schmelzer, I.; Smeed, D.A. Sea-level fluctuations during the last glacial cycle. *Nature* **2003**, *423*, 853–858. [[CrossRef](#)]
3. Lambeck, K.; Purcell, A. Sea-level change in the Mediterranean Sea since the LGM: Model predictions for tectonically stable areas. *Quat. Sci. Rev.* **2005**, *24*, 1969–1988. [[CrossRef](#)]
4. Rossi, V.; Amorosi, A.; Marchesini, M.; Marvelli, S.; Cocchianella, A.; Lorenzini, L.; Trigona, S.L.; Valle, G.; Bini, M. Late Quaternary Landscape Dynamics at the La Spezia Gulf (NW Italy): A Multi-Proxy Approach Reveals Environmental Variability within a Rocky Embayment. *Water* **2021**, *13*, 427. [[CrossRef](#)]

5. Morellón, M.; Anselmetti, F.S.; Ariztegui, D.; Brushulli, B.; Sinopoli, G.; Wagner, B.; Sadori, L.; Gilli, A.; Pambuku, A. Human-climate interactions in the central Mediterranean region during the last millennia: The laminated record of Lake Butrint (Albania). *Quat. Sci. Rev.* **2016**, *136*, 134–152. [[CrossRef](#)]
6. Di Rita, F.; Simone, O.; Caldara, M.; Gehrels, W.R.; Magri, D. Holocene environmental changes in the coastal Tavoliere Plain (Apulia, southern Italy): A multiproxy approach. *Palaeogeogr. Palaeoclimatol. Palaeoecol.* **2011**, *310*, 139–151. [[CrossRef](#)]
7. Miola, A.; Favaretto, S.; Sostizzo, I.; Valentini, G.; Asioli, A. Holocene salt marsh plant communities in the North Adriatic coastal plain (Italy) as reflected by pollen, non-pollen palynomorphs and plant macrofossil analyses. *Veg. Hist. Archaeobot.* **2010**, *19*, 513–529. [[CrossRef](#)]
8. Alday, M.; Cearreta, A.; Cachão, M.; Freitas, M.C.; Andrade, C.; Gama, C. Micropalaeontological record of Holocene estuarine and marine stages in the Corgo do Porto rivulet (Mira River, SW Portugal). *Estuar. Coast. Shelf Sci.* **2006**, *66*, 532–543. [[CrossRef](#)]
9. Triantaphyllou, M.V.; Pavlopoulos, K.; Tsourou, T.; Dermitzakis, M.D. Brackish marsh benthic microfauna and paleoenvironmental changes during the last 6000 years on the coastal plain of Marathon (SE Greece). *Riv. Ital. Paleontol. Stratigr.* **2003**, *109*, 539–547.
10. Hernández, A.; Cachão, M.; Sousa, P.; Trigo, R.M.; Luterbacher, J.; Vaquero, J.M.; Freitas, M.C. External forcing mechanisms controlling the North Atlantic coastal upwelling regime during the mid-Holocene. *Geology* **2020**, *49*, 433–437. [[CrossRef](#)]
11. Orefice, M.D.; Bellotti, P.; Bertini, A.; Calderoni, G.; Neri, P.C.; Di Bella, L.; Fiorenza, D.; Foresi, L.M.; Louvari, M.A.; Rainone, L.; et al. Holocene Evolution of the Burano Paleo-Lagoon (Southern Tuscany, Italy). *Water* **2020**, *12*, 1007. [[CrossRef](#)]
12. Pavlopoulos, K.; Kapsimalis, V.; Theodorakopoulou, K. Relative sea-level changes in Aegean coastal areas during Holocene: A geoarchaeological view. *J. Earth Sci.* **2010**, *21*, 244–246.
13. Avramidis, P.; Iliopoulos, G.; Nikolaou, K.; Kontopoulos, N.; Koutsodendris, A.; van Wijngaarden, G.J. Holocene sedimentology and coastal geomorphology of Zakynthos Island, Ionian Sea: A history of a divided Mediterranean island. *Palaeogeogr. Palaeoclimatol. Palaeoecol.* **2017**, *487*, 340–354. [[CrossRef](#)]
14. Vouvalidis, K.; Syrides, G.; Pavlopoulos, K.; Pechlivanidou, S.; Tsourlos, P.; Papakonstantinou, M.-F. Palaeogeographical reconstruction of the battle terrain in Ancient Thermopylae, Greece. *Geodin. Acta* **2010**, *23*, 241–253. [[CrossRef](#)]
15. Goiran, J.-P.; Pavlopoulos, K.P.; Fouache, E.; Triantaphyllou, M.V.; Etienne, R. Piraeus, the ancient island of Athens: Evidence from Holocene sediments and historical archives. *Geology* **2011**, *39*, 531–534. [[CrossRef](#)]
16. Pavlopoulos, K.; Theodorakopoulou, K.; Bassiakos, Y.; Hayden, B.; Tsourou, T.; Triantaphyllou, M.; Kouli, K.; Vandarakis, D. Paleoenvironmental evolution of Istron (N.E Crete), during the last 6000 years: Depositional environment, climate and sea level changes. *Geodin. Acta* **2007**, *20*, 219–229. [[CrossRef](#)]
17. Pavlopoulos, K.; Kapsimalis, V.; Theodorakopoulou, K.; Panagiotopoulos, I.P. Vertical displacement trends in the Aegean coastal zone (NE Mediterranean) during the Holocene assessed by geo-archaeological data. *Holocene* **2012**, *22*, 717–728. [[CrossRef](#)]
18. Pavlopoulos, K.; Karkanias, P.; Triantaphyllou, M.; Karymbalis, E.; Tsourou, T.; Palyvos, N. Paleoenvironmental evolution of the coastal plain of Marathon, Greece, during the Late Holocene: Depositional environment, climate, and sea level changes. *J. Coast. Res.* **2006**, *22*, 424–438. [[CrossRef](#)]
19. Kontopoulos, N.; Avramidis, P. A late Holocene record of environmental changes from the Alike lagoon, Egion, North Peloponnese, Greece. *Quat. Int.* **2003**, *111*, 75–90. [[CrossRef](#)]
20. Vött, A.; Schriever, A.; Handl, M.; Brückner, H. Holocene Palaeogeographies of the Eastern Acheloos River Delta and the Lagoon of Etoliko (NW Greece). *J. Coast. Res.* **2007**, *234*, 1042–1066. [[CrossRef](#)]
21. Evelpidou, N.; Pavlopoulos, K.; Vassilopoulos, A.; Triantaphyllou, M.V.; Vouvalidis, K.; Syrides, G. Yria (western Naxos island, Greece): Sea level changes in upper holocene and palaeogeographical reconstruction. *Geodin. Acta* **2010**, *23*, 233–240. [[CrossRef](#)]
22. Pavlopoulos, K.; Triantaphyllou, M.V.; Karkanias, P.; Kouli, K.; Syrides, G.; Vouvalidis, K.; Palyvos, N.; Tsourou, T. Paleoenvironmental evolution and prehistoric human environment, in the embayment of Palamari (Skyros Island, Greece) during Middle-Late Holocene. *Quat. Int.* **2010**, *216*, 41–53. [[CrossRef](#)]
23. Koukousioura, O.; Triantaphyllou, M.V.; Dimiza, M.D.; Pavlopoulos, K.; Syrides, G.; Vouvalidis, K. Benthic foraminiferal evidence and paleoenvironmental evolution of Holocene coastal plains in the Aegean Sea (Greece). *Quat. Int.* **2012**, *261*, 105–117. [[CrossRef](#)]
24. Syrides, G. Marine mollusk fauna and Holocene stratigraphy of the marsh of Agia Paraskevi, (Lamia, Fthiotida) Greece. *Bull. Geol. Soc. Greece* **2008**, *42*, 1–14.
25. Triantaphyllou, M.V.; Ziveri, P.; Gogou, A.; Marino, G.; Lykousis, V.; Bouloubassi, I.; Emeis, K.-C.C.; Kouli, K.; Dimiza, M.; Rosell-Melé, A.; et al. Late Glacial-Holocene climate variability at the south-eastern margin of the Aegean Sea. *Mar. Geol.* **2009**, *266*, 182–197. [[CrossRef](#)]
26. Triantaphyllou, M.V. Coccolithophore assemblages during the Holocene Climatic Optimum in the NE Mediterranean (Aegean and northern Levantine Seas, Greece): Paleooceanographic and paleoclimatic implications. *Quat. Int.* **2014**, *345*, 56–67. [[CrossRef](#)]
27. Marret, F.; Bradley, L.R.; Tarasov, P.E.; Ivanova, E.V.; Zenina, M.A.; Murdmaa, I.O. The Holocene history of the NE Black Sea and surrounding areas: An integrated record of marine and terrestrial palaeoenvironmental change. *Holocene* **2019**, *29*, 648–661. [[CrossRef](#)]
28. Kouli, K.; Brinkhuis, H.; Dale, B. *Spiniferites cruciformis*: A fresh water dinoflagellate cyst? *Rev. Palaeobot. Palynol.* **2001**, *113*, 273–286. [[CrossRef](#)]
29. Aksu, A.E.; Yaşar, D.; Mudie, P.J.; Gillespie, H. Late glacial-Holocene paleoclimatic and paleoceanographic evolution of the Aegean Sea: Micropaleontological and stable isotopic evidence. *Mar. Micropaleontol.* **1995**, *25*, 1–28. [[CrossRef](#)]

30. Mudie, P.J.; Aksu, A.E.; Yasar, D. Late Quaternary dinoflagellate cysts from the Black, Marmara and Aegean seas: Variations in assemblages, morphology and paleosalinity. *Mar. Micropaleontol.* **2001**, *43*, 155–178. [[CrossRef](#)]
31. Pavlopoulos, K.; Fouache, E.; Sidiropoulou, M.; Triantaphyllou, M.; Vouvalidis, K.; Syrides, G.; Gonnet, A.; Greco, E. Palaeoenvironmental evolution and sea-level changes in the coastal area of NE Lemnos Island (Greece) during the Holocene. *Quat. Int.* **2013**, *308–309*, 80–88. [[CrossRef](#)]
32. Triantaphyllou, M.V.; Kouli, K.; Tsourou, T.; Koukousioura, O.; Pavlopoulos, K.; Dermitzakis, M.D.D. Palaeoenvironmental changes since 3000 BC in the coastal marsh of Vravron (Attica, SE Greece). *Quat. Int.* **2010**, *216*, 14–22. [[CrossRef](#)]
33. Harff, J.; Flemming, N.C.; Groh, A.; Hünicke, B.; Lericolais, G.; Meschede, M.; Rosentau, A.; Sakellariou, D.; Uscinowicz, S.; Zhang, W.; et al. *Sea Level and Climate. In Submerged Landscapes of the European Continental Shelf: Quaternary Palaeoenvironments*; Flemming, N.C., Harff, J., Moura, D., Burgess, A., Bailey, G.N., Eds.; John Wiley & Sons Ltd.: Hoboken, NJ, USA, 2017; pp. 11–18. ISBN 9781118927823.
34. Galanidou, N.; Dellaporta, K.; Sakellariou, D. Greece: Unstable Landscapes and Underwater Archaeology. In *The Archaeology of Europe's Drowned Landscapes*; Springer: Cham, Switzerland, 2020; pp. 371–392. ISBN 9783030373672.
35. Lambeck, K.; Rouby, H.; Purcell, A.; Sun, Y.; Sambridge, M. Sea level and global ice volumes from the Last Glacial Maximum to the Holocene. *Proc. Natl. Acad. Sci. USA* **2014**, *111*, 15296–15303. [[CrossRef](#)]
36. Van Andel, T.H.; Zangger, E.; Perissoratis, C. Transgressive/Regressive Cycles in the Gulf of Argos, Greece. *Quat. Res.* **1990**, *34*, 317–329. [[CrossRef](#)]
37. Perissoratis, C.; Conispoliatis, N. The impacts of sea-level changes during latest Pleistocene and Holocene times on the morphology of the Ionian and Aegean seas (SE Alpine Europe). *Mar. Geol.* **2003**, *196*, 145–156. [[CrossRef](#)]
38. Karageorgis, A.P.; Kanellopoulos, T.D.; Mavromatis, V.; Anagnostou, C.L.; Koutsopoulou, E.; Schmidt, M.; Pavlopoulos, K.; Tripsanas, E.K.; Hallberg, R.O. Authigenic carbonate mineral formation in the Pagassitikos palaeolake during the latest Pleistocene, central Greece. *Geo-Mar. Lett.* **2013**, *33*, 13–29. [[CrossRef](#)]
39. McNeill, L.C.; Shillington, D.J.; Carter, G.D.O.; Everest, J.D.; Gawthorpe, R.L.; Miller, C.; Phillips, M.P.; Collier, R.E.L.; Cvetkoska, A.; De Gelder, G.; et al. High-resolution record reveals climate-driven environmental and sedimentary changes in an active rift. *Sci. Rep.* **2019**, *9*, 3116. [[CrossRef](#)]
40. Kapsimalis, V.; Pavlakakis, P.; Poulos, S.E.; Alexandri, S.; Tziavos, C.; Sioulas, A.; Filippas, D.; Lykousis, V. Internal structure and evolution of the Late Quaternary sequence in a shallow embayment: The Amvrakikos Gulf, NW Greece. *Mar. Geol.* **2005**, *222–223*, 399–418. [[CrossRef](#)]
41. Poulos, S.E.; Collins, M.B.; Lykousis, V. Late Quaternary Evolution of Amvrakikos Gulf, Western Greece. *Geo-Mar. Lett.* **1995**, *15*, 9–16. [[CrossRef](#)]
42. Perissoratis, C.; Piper, D.J.W.; Lykousis, V. Alternating marine and lacustrine sedimentation during late Quaternary in the Gulf of Corinth rift basin, central Greece. *Mar. Geol.* **2000**, *167*, 391–411. [[CrossRef](#)]
43. Petropoulos, A.; Androni, A.; Ntamkarelou, T.; Anagnostou, C. Carbonate and organic carbon content in the recent sediments of Elefsis bay as indicators for the palaeoenvironmental evolution of the system. *Bull. Geol. Soc. Greece* **2013**, *47*, 1562–1571. [[CrossRef](#)]
44. Foutrakis, P.M.; Anastasakis, G.; Piper, D.J.W. Chronology of Quaternary shoreline progradational sequences related to eustatic sea-level changes: Sedimentation and subsidence in Saronikos Gulf, Greece. *Mar. Geol.* **2020**, *428*, 106278. [[CrossRef](#)]
45. EC Directive of the European Parliament and of the Council 2000/60/EC establishing a framework for community action in the field of Water Policy. *J. Eur. Communities Bruss.* **2000**, *327*, 1–72.
46. Kersten, M.; Garbe-Schönberg, C.D.; Thomsen, S.; Anagnostou, C.; Sioulas, A. Source apportionment of Pb pollution in the coastal waters of Elefsis Bay, Greece. *Environ. Sci. Technol.* **1997**, *31*, 1295–1301. [[CrossRef](#)]
47. Karageorgis, A.P.; Botsou, F.; Kaberi, H.; Iliakis, S. Geochemistry of major and trace elements in surface sediments of the Saronikos Gulf (Greece): Assessment of contamination between 1999 and 2018. *Sci. Total Environ.* **2020**, *717*, 137046. [[CrossRef](#)]
48. Pavlidou, A.; Simboura, N.; Pagou, K.; Assimakopoulou, G.; Gerakaris, V.; Hatzianestis, I.; Panayotidis, P.; Pantazi, M.; Papadopoulou, N.; Reizopoulou, S.; et al. Using a holistic ecosystem-integrated approach to assess the environmental status of Saronikos Gulf, Eastern Mediterranean. *Ecol. Indic.* **2019**, *96*, 336–350. [[CrossRef](#)]
49. Kapetanaki, N.; Krasakopoulou, E.; Stathopoulou, E.; Dassenakis, M.; Scoullou, M. Severe coastal hypoxia interchange with ocean acidification: An experimental perturbation study on carbon and nutrient biogeochemistry. *J. Mar. Sci. Eng.* **2020**, *8*, 462. [[CrossRef](#)]
50. Primpas, I.; Tsirtsis, G.; Karydis, M.; Kokkoris, G.D. Principal component analysis: Development of a multivariate index for assessing eutrophication according to the European water framework directive. *Ecol. Indic.* **2010**, *10*, 178–183. [[CrossRef](#)]
51. Pavlidou, A.; Kontoyiannis, H.; Anagnostou, C.; Siokou-Frangou, I.; Pagou, K.; Krasakopoulou, E.; Assimakopoulou, G.; Zervoudaki, S.; Zeri, C.; Chatzianestis, J.; et al. *Biogeochemical Characteristics in the Elefsis Bay (Aegean Sea, Eastern Mediterranean) in Relation to Anoxia and Climate Changes BT—Chemical Structure of Pelagic Redox Interfaces: Observation and Modeling*; Yakushev, E.V., Ed.; Springer: Berlin/Heidelberg, Germany, 2013; pp. 161–201. ISBN 978-3-642-32125-2.
52. Dimiza, M.D.; Triantaphyllou, M.V.; Koukousioura, O.; Hallock, P.; Simboura, N.; Karageorgis, A.P.; Papatthanasidou, E. The Forum Stress Index: A new tool for environmental assessment of soft-bottom environments using benthic foraminifera. A case study from the Saronikos Gulf, Greece, Eastern Mediterranean. *Ecol. Indic.* **2016**, *60*, 611–621. [[CrossRef](#)]

53. Simboura, N.; Zenetos, A.; Pancucci-Papadopoulou, M.A. Benthic community indicators over a long period of monitoring (2000–2012) of the Saronikos Gulf, Greece, Eastern Mediterranean. *Environ. Monit. Assess.* **2014**, *186*, 3809–3821. [[CrossRef](#)] [[PubMed](#)]
54. *SoHelME State of the Marine Environment Report*; Papathanassiou, E.; Zenetos, A. (Eds.) HCMR Publisher: Athens, Greece, 2005; ISBN 9608665183.
55. Foutrakis, P.M.; Anastasakis, G. Quaternary continental shelf basins of Saronikos Gulf, Aegean Sea. *Geo-Mar. Lett.* **2020**, *40*, 629–647. [[CrossRef](#)]
56. Makris, J.; Papoulia, J.; Drakatos, G. Tectonic deformation and microseismicity of the Saronikos Gulf, Greece. *Bull. Seismol. Soc. Am.* **2004**, *94*, 920–929. [[CrossRef](#)]
57. Pantazidou, M.; Kapnariis, S.; Katsiri, A.; Christidis, A. Pollutant trends and hazard ranking in Elefsis Bay, Greece. *Desalination* **2007**, *210*, 69–82. [[CrossRef](#)]
58. Alexouli-Livaditi, A.; Livaditis, G.; Sachpazis, C. Geomorphological investigation of the drainage network and calculation of the peak storm runoff (Qp) and sediment yield of Sarantapotamos and Katsimidi streams, Attica, Greece. In *Proceedings of the Engineering Geology and the Environment*; Marinos, P.G., Koukis, G.C., Tsiambaos, G.C., Stournaras, G.C., Eds.; Balkema: Rotterdam, The Netherlands, 1997; pp. 31–40.
59. Lekkas, E. The Athens earthquake (7 September 1999): Intensity distribution and controlling factors. *Eng. Geol.* **2001**, *59*, 297–311. [[CrossRef](#)]
60. Friligos, N. Nutrient and oxygen redistribution during destratification in the Elefsis Bay, an anoxic basin. *Hydrobiologia* **1983**, *101*, 223–230. [[CrossRef](#)]
61. Siokou-Frangou, I.; Papathanassiou, E.; Lepretre, A.; Frontier, S. Zooplankton assemblages and influence of environmental parameters on them in a Mediterranean coastal area. *J. Plankton Res.* **1998**, *20*, 847–870. [[CrossRef](#)]
62. Scoullou, M.J.; Rilley, J. Water circulation in the Gulf of Elefsis, Greece. *Thalass. Jugosl.* **1978**, *14*, 357–370.
63. Pavlidou, A.; Pagou, K.; Assimakopoulou, G.; Rousselaki, E. Evolution over the last 30 years of the trophic conditions in the Gulf of Elefsis. In *Sustainable Mediterranean*; Issue No 71; Mediterranean Information Office for Environment, Culture and Sustainable Development, in collaboration with the European Environmental Bureau and the Arab NGO Network for Environment and Development: Athens, Greece, 2015; pp. 20–22.
64. Jiang, C.; Chen, Z.; Lavoie, D.; Percival, J.B.; Kabanov, P. Mineral carbon minC (%) from Rock-Eval analysis as a reliable and cost-effective measurement of carbonate contents in shale source and reservoir rocks. *Mar. Pet. Geol.* **2017**, *83*, 184–194. [[CrossRef](#)]
65. Facorellis, Y. Sea Surface radiocarbon reservoir age changes in the Aegean Sea from about 11,200 BP to present. *Radiocarbon* **2015**, *57*, 493–505. [[CrossRef](#)]
66. Reimer, P.; Bard, E.; Bayliss, A.; Beck, J.W.; Blackwell, P.G.; Ramsey, C.B.; Buck, C.E.; Cheng, H.; Edwards, R.L.; Friedrich, M.; et al. IntCal13 and Marine13 Radiocarbon Age Calibration Curves 0–50,000 Years cal BP. *Radiocarbon* **2013**, *55*, 1869–1887. [[CrossRef](#)]
67. Blaauw, M.; Christen, J.A.; Christen, A.J. Flexible paleoclimate age-depth models using an autoregressive gamma process. *Bayesian Anal.* **2011**, *6*, 457–474. [[CrossRef](#)]
68. Loeblich, A.R.; Tappan, H. *Foraminiferal Genera and Their Classification*; Van Nostrand Reinhold: New York, NY, USA, 1987.
69. Loeblich, A.R.; Tappan, H. *Foraminifera of the Sahul Shelf and Timor Sea*; Cushman Foundation for Foraminiferal Research: Washington, DC, USA, 1994; Volume 31.
70. Cimerman, F.; Langer, M. *Mediterranean Foraminifera*; Academia Scientiarum et Artium Slovenica: Ljubljana, Slovenia, 1991; Volume 30, Classis IV: Historia naturalis.
71. Hottinger, L.; Halicz, E.; Reiss, Z. *Recent Foraminiferida from the Gulf of Aqaba, Red Sea*; Academia Scientiarum et Artium Slovenica, Classis IV: Ljubljana, Slovenia, 1993; Volume 33.
72. Sgarrella, F.; Moncharmont-Zei, M. Benthic foraminifera of the Gulf of Naples (Italy): Systematics and autoecology. *Boll. Soc. Paleontol. Ital.* **1993**, *32*, 145–264.
73. Dimiza, M.D.; Koukousioura, O.; Triantaphyllou, M.V.; Dermitzakis, M.D. Live and dead benthic foraminiferal assemblages from coastal environments of the Aegean Sea (Greece): Distribution and diversity. *Rev. Micropaleontol.* **2016**, *59*, 19–32. [[CrossRef](#)]
74. Hammer, O.; Harper, D.A.T. *Paleontological Data Analysis*; Blackwell Publishing Ltd.: Hoboken, NJ, USA, 2006; ISBN 9781405115445.
75. Bonaduce, G.; Ciampo, G.; Masoli, M. Distribution of Ostracoda in the Adriatic Sea. *Pubblicazioni della Stazione zoologica di Napoli*; Napoli, Italy, 1975; Volume 40.
76. Stambolidis, E. Subrezente Ostracoden aus dem Evros-Delta (Griechenland) Einschliesslich der Entwicklung des Schlosses Gewisser Arten. *Acta Universitatis Upsaliensis*: Uppsala, Sweden, 1984.
77. Tsourou, T. Composition and Distribution of Recent Marine Ostracod Assemblages in the Bottom Sediments of Central Aegean Sea (SE Andros Island, Greece). *Int. Rev. Hydrobiol.* **2012**, *97*, 276–300. [[CrossRef](#)]
78. Tsourou, T.; Drinia, H.; Anastasakis, G. Ostracod assemblages from holocene middle shelf deposits of southern Evoikos gulf (Central Aegean Sea, Greece) and their palaeoenvironmental implications. *Micropaleontology* **2015**, *61*, 85–99.
79. Triantaphyllou, M.V.; Antonarakou, A.; Kouli, K.; Dimiza, M.; Kontakiotis, G.; Papanikolaou, M.D.D.; Ziveri, P.; Mortyn, P.G.G.; Lianou, V.; Lykousis, V.; et al. Late Glacial-Holocene ecostratigraphy of the south-eastern Aegean Sea, based on plankton and pollen assemblages. *Geo-Mar. Lett.* **2009**, *29*, 249–267. [[CrossRef](#)]

80. Flores, J.A.; Sierro, F.J.; Francés, G.; Vázquez, A.; Zamarreno, I. The last 100,000 years in the western Mediterranean: Sea surface water and frontal dynamics as revealed by coccolithophores. *Mar. Micropaleontol.* **1997**, *29*, 351–366. [CrossRef]
81. Triantaphyllou, M.V.; Antonarakou, A.; Dimiza, M.; Anagnostou, C. Calcareous nannofossil and planktonic foraminiferal distributional patterns during deposition of sapropels S6, S5 and S1 in the Libyan Sea (Eastern Mediterranean). *Geo-Mar. Lett.* **2010**, *30*, 1–13. [CrossRef]
82. Colmenero-Hidalgo, E.; Flores, J.-A.; Sierro, F.J.; Bárcena, M.Á.; Löwemark, L.; Schönfeld, J.; Grimalt, J.O. Ocean surface water response to short-term climate changes revealed by coccolithophores from the Gulf of Cadiz (NE Atlantic) and Alboran Sea (W Mediterranean). *Palaeogeogr. Palaeoclimatol. Palaeoecol.* **2004**, *205*, 317–336. [CrossRef]
83. Cros, L. Planktonic Coccolithophores of the NW Mediterranean. Ph.D. Thesis, Univ. de Barcelona, Barcelona, Spain, 2001.
84. Giraudeau, J. Distribution of recent nannofossils beneath the Benguela system: Southwest African continental margin. *Mar. Geol.* **1992**, *108*, 219–237. [CrossRef]
85. Dimiza, M.D.; Triantaphyllou, M.V.; Malinverno, E. New evidence for the ecology of *Helicosphaera carteri* in polluted coastal environments (Elefsis Bay, Saronikos, Greece). *J. Nannoplankt. Res.* **2014**, *34*, 37–43.
86. Dimiza, M.D.; Koukousioura, O.; Michailidis, I.; Dimou, V.G.; Navrozidou, V.; Aligizaki, K.; Seferlis, M. Seasonal living coccolithophore distribution in the enclosed coastal environments of the Thessaloniki Bay (Thermaikos Gulf, NW Aegean Sea). *Rev. Micropaleontol.* **2020**, *69*, 100449. [CrossRef]
87. Kyrikou, S.; Kouli, K.; Triantaphyllou, M.V.; Dimiza, M.D.; Gogou, A.; Panagiotopoulos, I.P.; Anagnostou, C.; Karageorgis, A.P. Late Glacial and Holocene vegetation patterns of Attica: A high-resolution record from Elefsis Bay, southern Greece. *Quat. Int.* **2020**, *545*, 28–37. [CrossRef]
88. Mudie, P.J.P.J.; Marret, F.; Mertens, K.N.; Shumilovskikh, L.; Leroy, S.A.G.G. Atlas of modern dinoflagellate cyst distributions in the Black Sea Corridor: From Aegean to Aral Seas, including Marmara, Black, Azov and Caspian Seas. *Mar. Micropaleontol.* **2017**, *134*, 1–152. [CrossRef]
89. Van Nieuwenhove, N.; Head, M.J.; Limoges, A.; Pospelova, V.; Mertens, K.N.; Matthiessen, J.; De Schepper, S.; de Vernal, A.; Eynaud, F.; Londeix, L.; et al. An overview and brief description of common marine organic-walled dinoflagellate cyst taxa occurring in surface sediments of the Northern Hemisphere. *Mar. Micropaleontol.* **2020**, *159*, 101814. [CrossRef]
90. Mudie, P.; Rochon, A.; Richards, K.; Ferguson, S.; Warny, S. *Spiniferites cruciformis*, *Pterocysta cruciformis* and *Galeacysta etrusca*: Morphology and palaeoecology. *Palynology* **2018**, *42*, 135–161. [CrossRef]
91. Mertens, K.N.; Ribeiro, S.; Bouimetarhan, I.; Caner, H.; Combourieu-Nebout, N.; Dale, B.; De Vernal, A.; Ellegaard, M.; Filipova, M.; Godhe, A.; et al. Process length variation in cysts of a dinoflagellate, *Lingulodinium machaerophorum*, in surface sediments: Investigating its potential as salinity proxy. *Mar. Micropaleontol.* **2009**, *70*, 54–69. [CrossRef]
92. Mertens, K.N.; Bradley, L.R.; Takano, Y.; Mudie, P.J.; Marret, F.; Aksu, A.E.; Hiscott, R.N.; Verleye, T.J.; Mousing, E.A.; Smyrnova, L.L.; et al. Quantitative estimation of Holocene surface salinity variation in the Black Sea using dinoflagellate cyst process length. *Quat. Sci. Rev.* **2012**, *39*, 45–59. [CrossRef]
93. WoRMs Database. Available online: www.marinespecies.org (accessed on 1 April 2021).
94. MSIP Database. Available online: www.species-identification.org (accessed on 1 April 2021).
95. Sakellariou, E. The Extant Molluscs of the Gulf of Thessaloniki and Their Contribution to Stratigraphy. Ph.D. Thesis, National and Kapodistrian University of Athens, Athens, Greece, 1957.
96. Gogou, A.; Bouloubassi, I.; Lykousis, V.; Arnaboldi, M.; Gaitani, P.; Meyers, P.A. Organic geochemical evidence of Late Glacial-Holocene climate instability in the North Aegean Sea. *Palaeogeogr. Palaeoclimatol. Palaeoecol.* **2007**, *256*, 1–20. [CrossRef]
97. Brassell, S.C.; Eglinton, G.; Marlowe, I.T.; Pflaumann, U.; Sarnthein, M. Molecular stratigraphy: A new tool for climatic assessment. *Nature* **1986**, *320*, 129–133. [CrossRef]
98. Conte, M.H.; Sicre, M.-A.; Rühlemann, C.; Weber, J.C.; Schulte, S.; Schulz-Bull, D.; Blanz, T. Global temperature calibration of the alkenone unsaturation index (UK'37) in surface waters and comparison with surface sediments. *Geochem. Geophys. Geosyst.* **2006**, *7*, Q02005. [CrossRef]
99. Eglinton, G.; Hamilton, R.J. Leaf epicuticular waxes. *Science* **1967**, *256*, 1322–1335. [CrossRef]
100. Ohkouchi, N.; Kawamura, K.; Kawahata, H.; Taira, A. Latitudinal distributions of terrestrial biomarkers in the sediments from the Central Pacific. *Geochim. Cosmochim. Acta* **1997**, *61*, 1911–1918. [CrossRef]
101. Poynter, J.G.; Farrimond, P.; Robinson, N.; Eglinton, G. *Aeolian-Derived Higher Plant Lipids in the Marine Sedimentary Record: Links with Palaeoclimate BT—Paleoclimatology and Paleometeorology: Modern and Past Patterns of Global Atmospheric Transport*; Leinen, M., Sarnthein, M., Eds.; Springer: Dordrecht, The Netherlands, 1989; pp. 435–462. ISBN 978-94-009-0995-3.
102. Apostolopoulos, G.; Pavlopoulos, K.; Goiran, J.-P.; Fouache, E. Was the Piraeus peninsula (Greece) a rocky island? Detection of pre-Holocene rocky relief with borehole data and resistivity tomography analysis. *J. Archaeol. Sci.* **2014**, *42*, 412–421. [CrossRef]
103. Tang, Z.; Cao, C.; Tang, K.; Qi, H.; Sun, Y.; Yang, J. Distribution of Carbon and Nitrogen as Indicators of Environmental Significance in Coastal Sediments of Weizhou Island, Beibu Gulf. *Water* **2020**, *12*, 3285. [CrossRef]
104. Nelson, S.A. Carbonates & Other Rocks. Available online: <http://www.tulane.edu/~sanelson/eens212/index.html> (accessed on 1 April 2021).
105. Guy-Holson, D. Botryococcus as an aid in the interpretation of palaeoenvironment and depositional processes. *Rev. Palaeobot. Palynol.* **1992**, *71*, 1–15. [CrossRef]

106. Mudie, P.J.; Leroy, S.A.G.; Marret, F.; Gerasimenko, N.P.; Kholeif, S.E.A.; Sapelko, T.; Filipova-Marinova, M. Nonpollen paly-nomorphs: Indicators of salinity and environmental change in the Caspian-Black Sea-Mediterranean corridor. *Spec. Pap. Geol. Soc. Am.* **2011**, *473*, 89–115.
107. Mariolakos, E.; Theochris, D. Shorelines displacement in the Saronic gulf area during the last 18,000 yrs and the Kihrea paleolake. *Bull. Geol. Soc. Greece* **2018**, *34*, 405–413. [[CrossRef](#)]
108. Roeser, P.; Franz, S.O.; Litt, T. Aragonite and calcite preservation in sediments from Lake Iznik related to bottom lake oxygenation and water column depth. *Sedimentology* **2016**, *63*, 2253–2277. [[CrossRef](#)]
109. Antczak, M. Palaeoecological significance of Late Glacial and Holocene molluscs. *Acta Biol.* **2014**, *21*, 5–21.
110. Soulié-Marsche, I. Charophytes, indicators for low salinity phases in North African sebkhet. *J. Afr. Earth Sci.* **2008**, *51*, 69–76. [[CrossRef](#)]
111. Murray, J.W. *Ecology and Applications of Benthic Foraminifera*; Cambridge University Press: Cambridge, UK, 2006.
112. Boltovskoy, E.; Giussani, G.; Watanabe, S.; Wright, R. *Atlas of Benthic Shelf Foraminifera to the Southwest Atlantic*; Dr. W. Junk by Publishers: The Hague, The Netherlands, 1980.
113. Melis, R.; Covelli, S. Distribution and morphological abnormalities of recent foraminifera in the Marano and Grado Lagoon (North Adriatic Sea, Italy). *Mediterr. Mar. Sci.* **2013**, *14*, 432–450. [[CrossRef](#)]
114. Boudreau, R.E.A.; Patterson, R.T.; Dalby, A.P.; McKillop, W.B. Non-marine occurrence of the foraminifer *Criboelphidium gunteri* in northern Lake Winnipegosis, Manitoba, Canada. *J. Foraminifer. Res.* **2001**, *31*, 108–119. [[CrossRef](#)]
115. Almogi-Labin, A.; Perelis-Grossovicz, L.; Raab, M. Living *Ammonia* from a hypersaline inland pool, Dead Sea area, Israel. *J. Foraminifer. Res.* **1992**, *22*, 257–266. [[CrossRef](#)]
116. Fatela, F.; Moreno, J.; Cabral, M.C. Salinity and water temperature assessment of the tidal marshes from the W Portuguese coast, as an ecological tool to palaeoenvironmental reconstructions based on foraminifera and ostracoda assemblages. *Estud. Quat.* **2016**, *14*, 73–81. [[CrossRef](#)]
117. Hohenegger, J.; Piller, W.; Baal, C. Reasons for Spatial Microdistributions of Foraminifers in an Intertidal Pool (Northern Adriatic Sea). *Mar. Ecol.* **1989**, *10*, 43–78. [[CrossRef](#)]
118. Poag, W.C. A Pilot Study of Paleocophenotypic Variation Among Quaternary Paralic Foraminifera in the USGS-Belle Fontaine No. 1 Core, Mississippi Gulf Coast. In *Stratigraphic and Paleontologic Studies of the Neogene and Quaternary Sediments in Southern Jackson County, Mississippi Chapter G*; U.S. Geological Survey: Reson, USA, 2001.
119. Neale, J.W. Ostracods and palaeosalinity reconstruction. In *Ostracoda Earth Sciences*; Elsevier: Amsterdam, The Netherlands, 1988; pp. 125–155.
120. Van Morkhoven, F.P.C.M.; van Morkhoven, F.P.C.M. *Post-Paleozoic Ostracoda: Their Morphology, Taxonomy and Economic Use*; Elsevier: Amsterdam, The Netherlands, 1962; Volume 1.
121. Keyser, D. Histological peculiarities of the nodding process in *Cyprideis torosa* (Jones) (Crustacea, Ostracoda). *Hydrobiologia* **2005**, *538*, 95–106. [[CrossRef](#)]
122. Frenzel, P.; Schulze, I.; Pint, A. Noding of *Cyprideis torosa* valves (Ostracoda)—A proxy for salinity? New data from field observations and a long-term microcosm experiment. *Int. Rev. Hydrobiol.* **2012**, *97*, 314–329. [[CrossRef](#)]
123. Rasmussen, S.O.; Bigler, M.; Blockley, S.P.; Blunier, T.; Buchardt, S.L.; Clausen, H.B.; Cvijanovic, I.; Dahl-Jensen, D.; Johnsen, S.J.; Fischer, H.; et al. A stratigraphic framework for abrupt climatic changes during the Last Glacial period based on three synchronized Greenland ice-core records: Refining and extending the INTIMATE event stratigraphy. *Quat. Sci. Rev.* **2014**, *106*, 14–28. [[CrossRef](#)]
124. Kotthoff, U.; Muller, U.C.; Pross, J.; Schmiedl, G.; Lawson, I.T.; van de Schootbrugge, B.; Schulz, H. Lateglacial and Holocene vegetation dynamics in the Aegean region: An integrated view based on pollen data from marine and terrestrial archives. *Holocene* **2008**, *18*, 1019–1032. [[CrossRef](#)]
125. Müller, U.C.; Pross, J.; Tzedakis, P.C.; Gamble, C.; Kotthoff, U.; Schmiedl, G.; Wulf, S.; Christanis, K. The role of climate in the spread of modern humans into Europe. *Quat. Sci. Rev.* **2011**, *30*, 273–279. [[CrossRef](#)]
126. Panagiotopoulos, K.; Aufgebauer, A.; Schäbitz, F.; Wagner, B. Vegetation and climate history of the Lake Prespa region since the Lateglacial. *Quat. Int.* **2013**, *293*, 157–169. [[CrossRef](#)]
127. Lawson, I.T.; Al-Omari, S.; Tzedakis, P.C.; Bryant, C.L.; Christanis, K. Lateglacial and Holocene vegetation history at Nisi Fen and the Boras mountains, northern Greece. *Holocene* **2005**, *15*, 873–887. [[CrossRef](#)]
128. Pope, R.J.; Hughes, P.D.; Skourtsos, E. Glacial history of Mt Chelmos, Peloponnesus, Greece. *Geol. Soc. Spec. Publ.* **2017**, *433*, 211–236. [[CrossRef](#)]
129. Hughes, P.D.; Woodward, J.C.; Gibbard, P.L. Quaternary glacial history of the Mediterranean mountains. *Prog. Phys. Geogr.* **2006**, *30*, 334–364. [[CrossRef](#)]
130. Leontaritis, A.D.D.; Kouli, K.; Pavlopoulos, K. The glacial history of Greece: A comprehensive review. *Mediterr. Geosci. Rev.* **2020**, *2*, 65–90. [[CrossRef](#)]
131. Allard, J.L.; Hughes, P.D.; Woodward, J.C.; Fink, D.; Simon, K.; Wilcken, K.M. Late Pleistocene glaciers in Greece: A new ³⁶Cl chronology. *Quat. Sci. Rev.* **2020**, *245*, 106528. [[CrossRef](#)]
132. Leroy, S.A.G.; Lahijani, H.A.K.; Reyss, J.L.; Chalié, F.; Haghani, S.; Shah-Hosseini, M.; Shahkarami, S.; Tudryn, A.; Arpe, K.; Habibi, P.; et al. A two-step expansion of the dinocyst *Lingulodinium machaerophorum* in the Caspian Sea: The role of changing environment. *Quat. Sci. Rev.* **2013**, *77*, 31–45. [[CrossRef](#)]

133. Zonneveld, K.A.F.; Marret, F.; Versteegh, G.J.M.; Bogus, K.; Bonnet, S.; Bouimetarhan, I.; Crouch, E.; de Vernal, A.; Elshanawany, R.; Edwards, L.; et al. Atlas of modern dinoflagellate cyst distribution based on 2405 data points. *Rev. Palaeobot. Palynol.* **2013**, *191*, 1–197. [[CrossRef](#)]
134. Leroy, S.A.G.; Albay, M. Palynomorphs of brackish and marine species in cores from the freshwater Lake Sapanca, NW Turkey. *Rev. Palaeobot. Palynol.* **2010**, *160*, 181–188. [[CrossRef](#)]
135. McNeill, L.C.; Shillington, D.J.; Carter, G.D.O.; Everest, J.D.; Le Ber, E.; Collier, R.E.; Cvetkoska, A.; De Gelder, G.; Diz, P.; Doan, M.L.; et al. Site M0078. In *Proceedings of the International Ocean Discovery Program*; International Ocean Discovery Program: Texas, USA, 2019; Volume 381.
136. Leroy, S.; Marret, F.; Gibert, E.; Chalie, F.; Reyss, J.-L.; Arpe, K. River inflow and salinity changes in the Caspian Sea during the last 5500 years. *Quat. Sci. Rev.* **2007**, *26*, 3359–3383. [[CrossRef](#)]
137. Debenay, J.P.; Millet, B.; Angelidis, M.O. Relationships between foraminiferal assemblages and hydrodynamics in the Gulf of Kalloni, Greece. *J. Foraminifer. Res.* **2005**, *35*, 327–343. [[CrossRef](#)]
138. Koukousioura, O.; Dimiza, M.D.; Kyriazidou, E.; Triantaphyllou, M.V.; Syrides, G.; Aidona, E.; Vouvalidis, K.; Panagiotopoulos, I.P.; Papadopoulou, L. Environmental evolution of the Paliouras coastal lagoon in the eastern Thermaikos gulf (Greece) during Holocene. *Environ. Earth Sci.* **2019**, *78*, 313. [[CrossRef](#)]
139. Pavlopoulos, K.; Triantaphyllou, M.V.; Karymbalis, E.; Karkanis, P.; Kouli, K.; Tsourou, T. Landscape evolution recorded in the embayment of Palamari (Skyros Island, Greece) from the beginning of the Bronze Age until recent times. *Géomorphol. Relief Process. Environ.* **2007**, *1*, 37–48. [[CrossRef](#)]
140. Dimou, V.-G.; Koukousioura, O.; Dimiza, M.D.; Triantaphyllou, M.V.; Less, G.; Pomoni-Papaioannou, F.; Syrides, G. A preliminary investigation of Eocene larger benthic foraminifera assemblages from Alpine and molasse-type deposits of the Hellenic peninsula (Greece). *Rev. Micropaleontol.* **2021**, *70*, 100468. [[CrossRef](#)]
141. Armynot Du Chatelet, E.; Degre, D.; Sauriau, P.-G.G.; Debenay, J.-P.P.; du Chatelet, E.A.; Degre, D.; Sauriau, P.-G.G.; Debenay, J.-P.P. Distribution of living benthic foraminifera in relation with environmental variables within the Aiguillon cove (Atlantic coast, France): Improving knowledge for paleoecological interpretation. *Bull. Soc. Géologique Fr.* **2009**, *180*, 131–144. [[CrossRef](#)]
142. Athersuch, J. The genus *Xestoleberis* with particular reference to Recent Mediterranean species. *Pubbl. Staz. Zool. Napoli* **1976**, *40*, 282–343.
143. Cronin, T.M.; Holmes, C.W.; Brewster-Wingard, G.L.; Ishman, S.E.; Dowsett, H.J.; Keyser, D.; Waibel, N. Historical trends in epiphytal ostracodes from Florida Bay: Implications for seagrass and macro-benthic algal variability. *Bull. Am. Paleontol.* **2001**, *361*, 159–197.
144. Viehberg, F.A.; Frenzel, P.; Hoffmann, G. Succession of late Pleistocene and Holocene ostracode assemblages in a transgressive environment: A study at a coastal locality of the southern Baltic Sea (Germany). *Palaeogeogr. Palaeoclimatol. Palaeoecol.* **2008**, *264*, 318–329. [[CrossRef](#)]
145. Athersuch, J. The ecology and distribution of the littoral ostracods of Cyprus. *J. Nat. Hist.* **1979**, *13*, 135–160. [[CrossRef](#)]
146. Cabral, M.C.; Freitas, M.C.; Andrade, C.; Cruces, A. Coastal evolution and Holocene ostracods in Melides lagoon (SW Portugal). *Mar. Micropaleontol.* **2006**, *60*, 181–204. [[CrossRef](#)]
147. Ruiz, F.; Abad, M.; Olías, M.; Galán, E.; González, I.; Aguilá, E.; Hamoumi, N.; Pulido, I.; Cantano, M. The present environmental scenario of the Nador Lagoon (Morocco). *Environ. Res.* **2006**, *102*, 215–229. [[CrossRef](#)] [[PubMed](#)]
148. Montenegro, M.E.; Pugliese, N.; Bonaduce, G. Shelf ostracods distribution in the Italian seas. In *What about Ostracoda! Proceedings of the 3rd European Ostracodologists Meeting, Bierville, France, 8–12 July 1996*; Crasquin-Soleau, S. S., Braccini, E., Lethiers, F., Eds.; Bullentin du Centre de Recherches Elf Exploration-Production Mémoire, 20: Pau, France, 1998; pp. 91–101.
149. Carboni, M.G.; Bergamin, L.; Di Bella, L.; Iamundo, F.; Pugliese, N. Palaeoecological evidences from foraminifers and ostracods on Late Quaternary sea-level changes in the Ombrone river plain (central Tyrrhenian coast, Italy). *Mem. Spec.* **2002**, *24*, 40–50.
150. Eisma, D. The influence of salinity on Mollusk shell mineralogy: A discussion. *J. Geol.* **1966**, *74*, 89–94. [[CrossRef](#)]
151. Tarnowska, K.; Wołowicz, M.; Chenuil, A.; Féral, J.P. Comparative studies on the morphometry and physiology of European populations of the lagoon specialist *Cerastoderma glaucum* (Bivalvia). *Oceanologia* **2009**, *51*, 437–458. [[CrossRef](#)]
152. Öztürk, B.; Poutiers, J.-M.; Musa Sari, H.; Özbek, M. On the occurrence of *Mytilaster marioni* (Locard, 1889) (Mollusca; Bivalvia; Mytilidae) in Bafa Lake (Turkey), with a redescription of the species. *Hydrobiologia* **2002**, *485*, 123–131. [[CrossRef](#)]
153. Fabbrocini, A.; Di Matteo, O.; D’Adamo, R. *Abra segmentum* (Mollusca: Pelecypoda) of the Lesina Lagoon (Southern Adriatic coast, Italy): Observations on variations in the population in relation to the main environmental parameters. *Transit. Waters Bull.* **2008**, *1*, 39–44.
154. Gontikaki, E.; Antoniadou, C.; Chintiroglou, C.C. Population structure of *Cerastoderma glaucum* and *Abra ovata* in Vouliagmeni Lagoon (Attiki). *J. Mar. Biol. Assoc. UK* **2003**, *83*, 1095–1097. [[CrossRef](#)]
155. Koukousioura, O.; Kouli, K.; Vouvalidis, K.; Aidona, E.; Karadimou, G.; Syrides, G. A multi-proxy approach for reconstructing environmental dynamics since the mid Holocene in Lake Ismarida (Thrace, N. Greece). *Rev. Micropaleontol.* **2020**, *68*, 100443. [[CrossRef](#)]
156. Nossier, M.A. Ecophysiological responses of *Cerastoderma edule* (L.) and *C. glaucum* (BRUGUIÈRE) to different salinity regimes and exposure to air. *J. Molluscan Stud.* **1986**, *52*, 110–119. [[CrossRef](#)]
157. Kevrekidis, T.; Gouvis, N.; Koukouras, A. Bionomy of Macrobenthic Molluscs in Evros Delta (North Aegean Sea). *Int. Rev. Ges. Hydrobiol.* **1996**, *81*, 455–468. [[CrossRef](#)]

158. Koutsoubas, D.; Arvanitidis, C.; Dounas, C.; Drummond, L. Community structure and dynamics of the Molluscan Fauna in a Mediterranean lagoon (Gialova lagoon, SW Greece). *Belg. J. Zool.* **2000**, *130*, 131–138.
159. Nicolaidou, A.; Bourgoutzani, F.; Zenetos, A.; Guelorget, O.; Perthuisot, J.-P.P. Distribution of molluscs and polychaetes in coastal lagoons in Greece. *Estuar. Coast. Shelf Sci.* **1988**, *26*, 337–350. [[CrossRef](#)]
160. Malham, S.K.; Hutchinson, T.H.; Longshaw, M. A review of the biology of European cockles (*Cerastoderma* spp.). *J. Mar. Biol. Assoc. UK* **2012**, *92*, 1563–1577. [[CrossRef](#)]
161. Colombani, N.; Osti, A.; Volta, G.; Mastrocicco, M. Impact of Climate Change on salinization of coastal water resources. *Water Resour. Manag.* **2016**, *30*, 2483–2496. [[CrossRef](#)]
162. Kouli, K.; Gogou, A.; Bouloubassi, I.; Triantaphyllou, M.V.V.; Ioakim, C.; Katsouras, G.; Roussakis, G.; Lykousis, V. Late postglacial paleoenvironmental change in the northeastern Mediterranean region: Combined palynological and molecular biomarker evidence. *Quat. Int.* **2012**, *261*, 118–127. [[CrossRef](#)]
163. Kouli, K.; Masi, A.; Mercuri, A.M.; Florenzano, A.; Sadori, L. Regional Vegetation Histories: An Overview of the Pollen Evidence from the Central Mediterranean. *Late Antiq. Archaeol.* **2018**, *11*, 69–82. [[CrossRef](#)]
164. Dormoy, I.; Peyron, O.; Combourieu-Nebout, N.; Goring, S.; Kotthoff, U.; Magny, M.; Pross, J. Terrestrial climate variability and seasonality changes in the Mediterranean region between 15,000 and 4000 years BP deduced from marine pollen records. *Clim. Past* **2009**, *5*, 615–632. [[CrossRef](#)]
165. Combourieu-Nebout, N.; Peyron, O.; Bout-Roumazelles, V.; Goring, S.; Dormoy, I.; Joannin, S.; Sadori, L.; Siani, G.; Magny, M. Holocene vegetation and climate changes in the central Mediterranean inferred from a high-resolution marine pollen record (Adriatic Sea). *Clim. Past* **2013**, *9*, 2023–2042. [[CrossRef](#)]
166. Aksu, A.E.; Abrajano, T.; Mudie, P.J.; Yaşar, D. Organic geochemical and palynological evidence for terrigenous origin of the organic matter in Aegean Sea sapropel S1. *Mar. Geol.* **1999**, *153*, 303–318. [[CrossRef](#)]
167. Morzadec-Kerfourn, M.T. Interaction between sea-level changes and the development of littoral herbaceous vegetation and autotrophic dinoflagellates. *Quat. Int.* **2005**, *133–134*, 137–140. [[CrossRef](#)]
168. Dimiza, M.D.; Triantaphyllou, M.V.; Dermitzakis, M.D. Seasonality and ecology of living coccolithophores in Eastern Mediterranean coastal environments (Andros Island, Middle Aegean Sea). *Micropaleontology* **2008**, *54*, 159–175.
169. Mouffi-El-Houari, L.; Ambroise, D.; Mathieu, R. Distribution des foraminifères benthiques actuels sur la marge continentale Algéroise (Baie De Bou-Ismaïl). *Rev. Micropaleontol.* **1999**, *42*, 315–327. [[CrossRef](#)]
170. Jorissen, F.J. The distribution of benthic foraminifera in the Adriatic Sea. *Mar. Micropaleontol.* **1987**, *12*, 21–48. [[CrossRef](#)]
171. Langer, M.R. Epiphytic foraminifera. *Mar. Micropaleontol.* **1993**, *20*, 235–265. [[CrossRef](#)]
172. Boomer, I.; Guichard, P.; Lericolais, G. Late Pleistocene to Recent ostracod assemblages from the western Black Sea. *J. Micropaleontol.* **2010**, *29*, 119–133. [[CrossRef](#)]
173. Frezza, V.; Di Bella, L. Distribution of recent ostracods near the Ombrone River mouth (Northern Tyrrhenian Sea, Italy). *Micropaleontology* **2015**, *61*, 101–114.
174. Barbieri, G.; Rossi, V.; Vaiani, S.C.; Horton, B.P. Benthic ostracoda and foraminifera from the North Adriatic Sea (Italy, Mediterranean Sea): A proxy for the depositional characterisation of river-influenced shelves. *Mar. Micropaleontol.* **2019**, *153*, 101772. [[CrossRef](#)]
175. Heusser, L.; Balsam, W.L. Pollen Distribution in the Northeast Pacific Ocean. *Quat. Res.* **1977**, *7*, 45–62. [[CrossRef](#)]
176. Mudie, P.J. Pollen distribution in recent marine sediments, eastern Canada. *Can. J. Earth Sci.* **1982**, *19*, 729–747. [[CrossRef](#)]
177. De Vernal, A. Palynology (Pollen, Spores, etc.). In *Encyclopedia of Marine Geosciences*; Springer Science + Business Media: Dordrecht, The Netherlands, 2015; pp. 1–9. ISBN 9789400766440.
178. Naughton, F.; Sanchez Goñi, M.F.; Desprat, S.; Turon, J.L.; Duprat, J.; Malaizé, B.; Joli, C.; Cortijo, E.; Drago, T.; Freitas, M.C. Present-day and past (last 25,000 years) marine pollen signal off western Iberia. *Mar. Micropaleontol.* **2007**, *62*, 91–114. [[CrossRef](#)]
179. Gogou, A.; Triantaphyllou, M.V.; Xoplaki, E.; Izdebski, A.; Parinos, C.; Dimiza, M.; Bouloubassi, I.; Luterbacher, J.; Kouli, K.; Martrat, B.; et al. Climate variability and socio-environmental changes in the northern Aegean (NE Mediterranean) during the last 1500 years. *Quat. Sci. Rev.* **2016**, *136*, 209–228. [[CrossRef](#)]
180. Mercuri, A.M.; Mazzanti, M.B.; Torri, P.; Vigliotti, L.; Bosi, G.; Florenzano, A.; Olmi, L.; N’siala, I.M. A marine/terrestrial integration for mid-late Holocene vegetation history and the development of the cultural landscape in the Po valley as a result of human impact and climate change. *Veg. Hist. Archaeobot.* **2012**, *21*, 353–372. [[CrossRef](#)]
181. Sadori, L.; Koutsodendris, A.; Masi, A.; Bertini, A.; Combourieu-Nebout, N.; Francke, A.; Kouli, K.; Joannin, S.; Mercuri, A.M.; Panagiotopoulos, K.; et al. Pollen-based paleoenvironmental and paleoclimatic change at Lake Ohrid (SE Europe) during the past 500 ka. *Biogeosciences* **2016**, *13*, 1423–1437. [[CrossRef](#)]
182. Panagiotopoulos, K.; Holtvoeth, J.; Kouli, K.; Marinova, E.; Francke, A.; Cvetkoska, A.; Jovanovska, E.; Lacey, J.H.; Lyons, E.T.; Buckel, C.; et al. Insights into the evolution of the young Lake Ohrid ecosystem and vegetation succession from a southern European refugium during the Early Pleistocene. *Quat. Sci. Rev.* **2020**, *227*, 106044. [[CrossRef](#)]
183. Sadori, L. The Lateglacial and Holocene vegetation and climate history of Lago di Mezzano (central Italy). *Quat. Sci. Rev.* **2018**, *202*, 30–44. [[CrossRef](#)]
184. Triantaphyllou, M.V.; Gogou, A.; Bouloubassi, I.; Dimiza, M.; Kouli, K.; Rousakis, G.; Kotthoff, U.; Emeis, K.C.; Papanikolaou, M.; Athanasiou, M.; et al. Evidence for a warm and humid Mid-Holocene episode in the Aegean and northern Levantine Seas (Greece, NE Mediterranean). *Reg. Environ. Chang.* **2014**, *14*, 1697–1712. [[CrossRef](#)]

185. Cullen, H.M.; DeMenocal, P.B.; Hemming, S.; Hemming, G.; Brown, F.H.; Guilderson, T.; Sirocko, F. Climate change and the collapse of the Akkadian empire: Evidence from the deep sea. *Geology* **2000**, *28*, 379. [[CrossRef](#)]
186. Finné, M.; Holmgren, K.; Sundqvist, H.S.; Weiberg, E.; Lindblom, M. Climate in the eastern Mediterranean, and adjacent regions, during the past 6000 years—A review. *J. Archaeol. Sci.* **2011**, *38*, 3153–3173. [[CrossRef](#)]
187. Marret, F.; Zonneveld, K.A.F. Atlas of modern organic-walled dinoflagellate cyst distribution. *Rev. Palaeobot. Palynol.* **2003**, *125*, 1–200. [[CrossRef](#)]
188. Peyron, O.; Combourieu-Nebout, N.; Brayshaw, D.; Goring, S.; Andrieu-Ponel, V.; Desprat, S.; Fletcher, W.; Gambin, B.; Ioakim, C.; Joannin, S.; et al. Precipitation changes in the Mediterranean basin during the Holocene from terrestrial and marine pollen records: A model–data comparison. *Clim. Past* **2017**, *13*, 249–265. [[CrossRef](#)]
189. Roberts, N.; Eastwood, W.J.; Kuzucuoglu, C.; Fiorentino, G.; Caracuta, V. Climatic, vegetation and cultural change in the eastern Mediterranean during the mid-Holocene environmental transition. *Holocene* **2011**, *21*, 147–162. [[CrossRef](#)]
190. Sadori, L.; Jahns, S.; Peyron, O. Mid-Holocene vegetation history of the central Mediterranean. *Holocene* **2011**, *21*, 117–129. [[CrossRef](#)]
191. Barmawidjaja, D.M.; Jorissen, F.J.; Puskaric, S.; van der Zwaan, G.J. Microhabitat selection by benthic foraminifera in the northern Adriatic Sea. *J. Foraminifer. Res.* **1992**, *22*, 297–317. [[CrossRef](#)]
192. Jorissen, F.J.; Barmawidjaja, D.M.; Puskaric, S.; van der Zwaan, G.J. Vertical distribution of benthic foraminifera in the northern Adriatic Sea: The relation with the organic flux. *Mar. Micropaleontol.* **1992**, *19*, 131–146. [[CrossRef](#)]
193. Goineau, A.; Fontanier, C.; Mojtahid, M.; Fanget, A.S.; Bassetti, M.A.; Berné, S.; Jorissen, F. Live-dead comparison of benthic foraminiferal faunas from the Rhône prodelta (Gulf of Lions, NW Mediterranean): Development of a proxy for palaeoenvironmental reconstructions. *Mar. Micropaleontol.* **2015**, *119*, 17–33. [[CrossRef](#)]
194. Moodley, L.; Heip, C.H.R.; Middelburg, J.J. Benthic activity in sediments of the northwestern Adriatic Sea: Sediment oxygen consumption, macro- and meiofauna dynamics. *J. Sea Res.* **1998**, *40*, 263–280. [[CrossRef](#)]
195. Bernhard, J.M.; Sen Gupta, B.K. Foraminifera in oxygen-depleted environments. In *Modern Foraminifera*; Sen Gupta, B.K., Ed.; Kluwer: Dordrecht, The Netherlands, 1999; pp. 201–216.
196. Diaz, R.J.; Rosenberg, R. Marine benthic hypoxia: A review of its ecological effects and the behavioural responses of benthic macrofauna. *Oceanogr. Mar. Biol. Annu. Rev.* **1995**, *33*, 245–303.
197. Jensen, J.N. Increased abundance and growth of the suspension-feeding bivalve *Corbula gibba* in a shallow part of the eutrophic Limfjord, Denmark. *Neth. J. Sea Res.* **1990**, *27*, 101–108. [[CrossRef](#)]
198. Wilding, T.A. The Benthic Impacts of the Loch Linnhe Artificial Reef. *Hydrobiologia* **2006**, *555*, 345–353. [[CrossRef](#)]
199. Büyükmeriç, Y.; Wesselingh, F.P.; Alçiçek, M.C. Middle–late Pleistocene marine molluscs from Izmit Bay area (eastern Marmara Sea, Turkey) and the nature of Marmara—Black Sea corridors. *Quat. Int.* **2016**, *401*, 153–161. [[CrossRef](#)]
200. Triantaphyllou, M. Coccolithophores—And related taxa—In the modern oceans. *Rev. Micropaleontol.* **2016**, *59*, 225. [[CrossRef](#)]